

Chemical characterization and source apportionment of fine particulate matter in ~~Eastern Africa~~ Kigali, Rwanda, using aerosol mass spectrometry.

Theobard Habineza¹, Allen L. Robinson², H. Langley DeWitt³, Jimmy Gasore⁴, Philip L. Croteau⁵, Albert A. Presto^{*1,4}

5

¹Carnegie Mellon University, Department of Mechanical Engineering and Center for Atmospheric Particle Studies (CAPS)

²Department of Atmospheric Science, Colorado State University

10 ³CIRES, University of Colorado, Boulder, CO, USA

⁴ Kigali Collaborative Research Center, Kigali, Rwanda

⁵Aerodyne Research, Inc., Billerica, Massachusetts, USA

*Corresponding author: apresto@andrew.cmu.edu

15 **Abstract**

Ambient air pollution poses a significant threat to public health, particularly in low and middle-income countries, where detailed data on particulate matter (PM) mass and composition are scarce. We conducted a year-long study on PM composition and sources in Eastern Africa (Kigali, Rwanda). The annual mean concentration of PM₁ was 31±15 μg/m³, with slightly higher concentrations during the dry season. Organic aerosols (OA) contributed 73% of the observed PM₁ mass, black carbon (BC) 16%, nitrate 6%, sulfate and ammonium 2% each, and chlorine 1%. BC is approximately 60% due to fossil fuel emissions and 40% from biomass burning emissions. Tracer ions detected by the [aerosol](#) mass spectrometer suggest that photochemistry plays a significant role in the formation of secondary OA during the daytime (6:00 am to 6:00 pm), while primary OA dominates in the morning and evening due to increased anthropogenic activity and shallower boundary layer height. PM₁ [OA](#) in Kigali is primarily composed of Oxygenated Organic Aerosols (OOA, 45%), Hydrocarbon-like OA (HOA, 32%), and Biomass Burning OA (BBOA, 23%). Secondary organic aerosol (SOA) accounted for 47% and 41% of PM₁ [OA](#) during the rainy and

25

dry seasons, respectively, while primary OA (POA: BBOA + HOA) contributed 53% and 59%. This suggests that seasonal changes in PM₁ mass in Kigali are primarily driven by deposition, chemical production, and source strength rather than shifts in primary emissions. Short-term interventions that limit traffic activity on some Saturdays and Sundays had a mixed impact on ambient PM₁ and PM_{2.5} concentrations, with car-free Sundays reducing PM₁ concentrations throughout most of the day, rather than shifts in emissions, chemical processing, or source strengths.

Formatted: Subscript

Formatted: Subscript

Formatted: Subscript

35

1. Introduction

Air pollution exposure has severe impacts on public health. Air pollution is classified as the second leading risk factor for deaths in Africa (Health Effects Institute, 2022). The adverse effects of air pollution manifest as cardiovascular diseases, respiratory diseases, and cerebrovascular diseases (Brito *et al.*, 2018; Health Effects Institute, 2023; WHO, 2025). In 2019, ambient air pollution was estimated to cause 4.2 million premature deaths globally, with 89% occurring in low- and middle-income countries (LMICs), including 1.1 million deaths in Africa (UN Environment, 2019; Subramanian *et al.*, 2020; WHO, 2025). Studies in the Global South, including Eastern Africa, have revealed that particulate matter (PM), defined as solid or liquid particles suspended in the air, is the air pollutant most responsible for human health impacts and a leading risk factor across sub-Saharan Africa (SSA) (Health Effects Institute, 2022). PM mass concentrations in Africa often reach unhealthy levels compared to the World Health Organization's (WHO) air quality guidelines, posing significant health risks to public health and the environment (Gaita *et al.*, 2014; Andersson *et al.*, 2020; Singh *et al.*, 2021; Onyango *et al.*, 2024). Rapid population growth, urbanization, energy consumption, and motorization have been reported as drivers of air pollution in LMICs (Brito *et al.*, 2018; REMA, 2018; Tefera *et al.*, 2021; Health Effects Institute, 2022). Eastern Africa and the Global South, in general, face a noticeable scarcity of air pollution measurements (AirNow, 2025; openaq, 2025). This hinders the understanding of air pollution impacts. Developing effective regulatory strategies requires information on air pollutant sources, which in turn requires

Formatted: Font: (Default) Times New Roman, Font color: Black, English (United Kingdom), Ligatures: None

Formatted: Font: (Default) Times New Roman, Font color: Black, English (United Kingdom), Ligatures: None

Formatted: Font: (Default) Times New Roman, Font color: Black, English (United Kingdom), Ligatures: None

Formatted: Font: (Default) Times New Roman, Font color: Black, English (United Kingdom), Ligatures: None

Formatted: Font: (Default) Times New Roman, Font color: Black, Italian (Italy), Ligatures: None

Formatted: Font: (Default) Times New Roman, Font color: Black, English (United Kingdom), Ligatures: None

Formatted: Font: (Default) Times New Roman, Font color: Black, English (United Kingdom), Ligatures: None

Formatted: Font: (Default) Times New Roman, Font color: Black, English (United Kingdom), Ligatures: None

Formatted: Font: (Default) Times New Roman, Font color: Black, English (United Kingdom), Ligatures: None

55 measurements of PM composition. The data gaps are even larger for PM composition measurements than
for PM mass concentrations (Dhammapala, 2019).
The few published studies on air pollution in Eastern Africa showed that PM concentrations exceed the
World Health Organization (WHO) guidelines (REMA, 2018; McFarlane *et al.*, 2021; Gahungu and
Kubwimana, 2022; Ndamuzi *et al.*, 2024; Onyango *et al.*, 2024; Kalisa *et al.*, 2025), and higher
concentrations of PM_{2.5} (particulate matter smaller than 2.5 microns in diameter) are present in urban
60 areas (Health Effects Institute, 2022). PM_{2.5} concentrations in eastern African cities are 3 to >10 times
higher than the 5 µg/m³ air quality guidelines (AQG) set forth by the World Health Organization (Health
Effects Institute, 2022). Gahungu and Kubwimana (Gahungu and Kubwimana, 2022) used low-cost
sensors and found that the daily mean concentration of PM_{2.5} in Kigali, Rwanda, was approximately 30
µg/m³ in the rainy season and 55 µg/m³ in the dry season. Kalisa *et al.* measured hourly average PM_{2.5}
65 concentrations of 25 µg/m³ in the city center of Kigali (Kalisa *et al.*, 2018). Onyango *et al.*, using US
State Department PM_{2.5} monitor data and filter collection, reported that the mean PM_{2.5} in Kampala,
Uganda, is 59.4 µg/m³ (Onyango *et al.*, 2024). McFarland *et al.* reported mean PM_{2.5} concentrations of
43.5 µg/m³ in the central African city of Kinshasa, Democratic Republic of Congo (DRC) (McFarlane *et al.*,
et al., 2021). Ndamuzi *et al.*, using low-cost sensors coupled with mathematical models, reported an annual
70 mean PM_{2.5} of 35.0 µg/m³ in Bujumbura, Burundi (Ndamuzi *et al.*, 2024).
Data on PM composition and sources are scarce. While Some composition information comes from the
Rwanda Climate Observatory, a remote site outside Kigali (Kirago *et al.*, 2022). Within Kigali, studies
have reported BC, PAHs, and NPAHs (Kalisa *et al.*, 2018, 2025; Subramanian *et al.*, 2020; Kalisa and
Adams, 2022), but no detailed PM composition data have been reported for the city itself.
75 There is limited information on PM composition and sources in Eastern Africa. Studies on PM_{2.5} chemical
speciation and source apportionment in Eastern Africa identified traffic emissions (36%) and
biomass/secondary aerosols (28%) as the main sources of PM_{2.5} in Mbarara, Uganda (Onyango *et al.*
2024b), while mineral dust and traffic emissions together account for 74% of PM_{2.5} in Nairobi, Kenya
80 (Gaita *et al.* 2014). The chemical composition and sources of PM_{2.5} in other Eastern African cities are still
unexplored, and without detailed data on PM composition, source identification remains unknown.

Formatted: Font: (Default) Times New Roman, Font color: Black, English (United Kingdom), Ligatures: None

Formatted: Font: (Default) Times New Roman, Font color: Black, English (United Kingdom), Ligatures: None

Formatted: Font: (Default) Times New Roman, Font color: Black, English (United Kingdom), Ligatures: None

Formatted: Font: (Default) Times New Roman, Font color: Black, English (United Kingdom), Ligatures: None

Formatted: Font: (Default) Times New Roman, Font color: Black, English (United Kingdom), Ligatures: None

Formatted: Font: (Default) Times New Roman, Font color: Black, English (United Kingdom), Ligatures: None

Formatted: Font: (Default) Times New Roman, Font color: Black, English (United Kingdom), Ligatures: None

Formatted: Font: (Default) Times New Roman, Font color: Black, English (United Kingdom), Ligatures: None

Formatted: Font: (Default) Times New Roman, Font color: Black, English (United Kingdom), Ligatures: None

Formatted: Font: (Default) Times New Roman, Font color: Black, English (United Kingdom), Ligatures: None

Formatted: Font: (Default) Times New Roman, Font color: Black, English (United Kingdom), Ligatures: None

Formatted: Font: (Default) Times New Roman, Font color: Black, English (United Kingdom), Ligatures: None

Formatted: Font: (Default) Times New Roman, Font color: Black, English (United Kingdom), Ligatures: None

Formatted: Font: (Default) Times New Roman, Font color: Black, English (United Kingdom), Ligatures: None

Formatted: Font: Not Bold

Formatted: Font: (Default) Times New Roman, Font color: Black, English (United Kingdom), Ligatures: None

Formatted: Font: (Default) Times New Roman, Font color: Black, English (United Kingdom), Ligatures: None

Formatted: Font: (Default) Times New Roman, Font color: Black, English (United Kingdom), Ligatures: None

Formatted: Font: (Default) Times New Roman, Font color: Black, English (United Kingdom), Ligatures: None

Formatted: Font: (Default) Times New Roman, Font color: Black, English (United Kingdom), Ligatures: None

Rwanda, an Eastern African country, is experiencing rapid population growth in its urban centers, particularly in its capital city, Kigali. The annual rate of urbanization is 4.1%, contributing to a high population density of 2,330 inhabitants per km² as of 2023 (Kigali city, 2024). Notably, 85% of households in Kigali rely on biomass burning for cooking, which includes wood, charcoal, and waste materials (MINEFRA, 2015, 2018b). Additionally, 13% of households use petroleum-based fuels such as diesel, kerosene, and liquified petroleum gas (LPG) (MINEFRA, 2018b; UNFCCC Rwanda, 2021). In 2019, air pollution-related deaths in Rwanda were estimated at 9,286, and an estimated economic cost of \$349 million (Fisher *et al.*, 2021) following a rise of 41% from 2008 to 2019 (GBD, 2024; Taghian *et al.*, 2024).

Governments are deploying a range of policies to curb air pollution and its impacts. In Rwanda, the transport sector is targeting traffic-related PM by discouraging imports of vehicles older than 20 years and advancing electric-mobility policies (Rwanda, 2021). Demand-side measures, including car-free days and nationwide community work (Umuganda), further reduce traffic during peak windows. In the industrial and energy sectors, Rwanda is aligning with East African Community (EAC) emission standards, EAS 750:2010 (ambient air), EAC 751:2010 (cement factories), and EAC 1047:2022 (tailpipe emissions) and expanding access to low-emission cookstoves in rural communities to cut household PM (Republic of Rwanda, 2022).

ountries are

To better understand PM chemical composition, concentration, and sources in Eastern Africa, we conducted long-term ground measurements of PM mass concentration and chemical composition using an aerosol mass spectrometer at a central site in Kigali, Rwanda. This study uses a 12-month (April 2023 to May 2024) dataset that captures the four alternating rainy and dry seasons in Rwanda and Eastern Africa in general. These data represent the first mass spectrometry-based PM composition measurements in the region, offering high-time resolution insights. The findings not only enhance an understanding of PM composition but also provide a vital tool for policymakers to develop data-driven air pollution mitigation strategies and targeted interventions in this region.

Formatted: Font: (Default) Times New Roman, Font color: Black, English (United Kingdom), Ligatures: None

Formatted: Font: (Default) Times New Roman, Font color: Black, English (United Kingdom), Ligatures: None

Formatted: Font: (Default) Times New Roman, Font color: Black, English (United Kingdom), Ligatures: None

Formatted: Font: (Default) Times New Roman, Font color: Black, English (United Kingdom), Ligatures: None

Formatted: Font: (Default) Times New Roman, Font color: Black, English (United Kingdom), Ligatures: None

Formatted: Font: (Default) Times New Roman, Font color: Black, English (United Kingdom), Ligatures: None

Formatted: Font: (Default) Times New Roman, Font color: Black, English (United Kingdom), Ligatures: None

Formatted: Font: (Default) Times New Roman, Font color: Black, English (United Kingdom), Ligatures: None

Formatted: Font: (Default) Times New Roman, Font color: Black, English (United Kingdom), Ligatures: None

Formatted: Font: (Default) Times New Roman, Font color: Black, English (United Kingdom), Ligatures: None

Formatted: Default Paragraph Font, Font: (Default) Times New Roman, Font color: Black, English (United Kingdom), Ligatures: None

Formatted: Font: (Default) Times New Roman, Font color: Black, English (United Kingdom), Ligatures: None

Formatted: Font: (Default) Times New Roman, Font color: Black, English (United Kingdom), Ligatures: None

Formatted: Font: (Default) Times New Roman, Font color: Black, English (United Kingdom), Ligatures: None

2. Methods

2.1 Sampling location

Real-time PM₁ data were collected from April 2023 to May 2024 at a fixed monitoring station located at the University of Rwanda, College of Science and Technology (UR/CST) at latitude -1.9619, longitude 30.0645 in Nyarugenge District, Kigali City (Figure S1, Supporting Information).

Kigali is characterized by rolling hills, with steep slopes connecting a network of valleys and ridges at an altitude of approximately 1,500 meters above sea level (Meteo_Rwanda, 2025). The monitoring site is in the city center, on the third floor of a three-story building at UR/CST. The site is surrounded by a mix of commercial and residential neighborhoods, with busy roads in the city center in Nyarugenge District, making it representative of an urban background station.

Like many Eastern African cities, Kigali experiences four alternating seasons: the long dry season (June, July, and August), the short rainy season (September, October, and November), the short dry season (December, January, and February), and the long rainy season (March, April, and May). The terms “short” and “long” refer to the intensity and consistency of rainfall and sunshine, rather than their duration (Nicholson, 2017). The annual average rainfall in Kigali is 1170 mm, the annual mean temperature is 22 °C, and the annual maximum temperature is 33 °C (World Bank, 2021; Kigali city, 2024).

Kigali City is experiencing rapid urbanization with a population of 1,745,555 inhabitants (Kigali city, 2024), leading to an increase in traffic and frequent traffic congestion. As of 2018, the vehicle fleet in Kigali was dominated by imported used vehicles, with 95.2% of the total fleet being older than 10 years (Miller and Jin, 2018; UN Environment, 2019).

2.2 In-situ measurements of PM and BC

A quadrupole Aerosol Chemical Speciation Monitor (Q-ACSM) from Aerodyne Research was used to measure the ambient concentration and composition of non-refractory PM₁ (NR-PM₁) in real-time (Ng et al., 2011). The ACSM uses aerosol mass spectrometry to speciate NR-PM₁ components, including organic aerosol (Org), sulfate (SO₄), nitrate (NO₃), ammonium (NH₄), and chloride (Cl). During sampling, ambient air is sampled through an inlet line equipped with a 1 μm cyclone to remove larger

Formatted: Font: (Default) Times New Roman, Bold, English (United Kingdom), Ligatures: None

Formatted: Font: (Default) Times New Roman, Font color: Black, English (United Kingdom), Ligatures: None

Formatted: Font: (Default) Times New Roman, Font color: Black, English (United Kingdom), Ligatures: None

Formatted: Font: (Default) Times New Roman, Font color: Black, English (United Kingdom), Ligatures: None

Formatted: Font: (Default) Times New Roman, Font color: Black, English (United Kingdom), Ligatures: None

Formatted: Font: (Default) Times New Roman, Font color: Black, English (United Kingdom), Ligatures: None

Formatted: Font: (Default) Times New Roman

Formatted: Font: (Default) Times New Roman, Font color: Black, English (United Kingdom), Ligatures: None

Formatted: Font: (Default) Times New Roman, Font color: Black, English (United Kingdom), Ligatures: None

Formatted: Font: (Default) Times New Roman, Font color: Black, English (United Kingdom), Ligatures: None

Formatted: Font: (Default) Times New Roman, Font color: Black, English (United Kingdom), Ligatures: None

Formatted: Font: (Default) Times New Roman, Font color: Black, English (United Kingdom), Ligatures: None

Formatted: Font: (Default) Times New Roman, Font color: Black, English (United Kingdom), Ligatures: None

Formatted: Font: (Default) Times New Roman, Font color: Black, English (United Kingdom), Ligatures: None

Formatted: Font: (Default) Times New Roman, English (United Kingdom), Ligatures: None

Formatted: Font: (Default) Times New Roman, Font color: Black, English (United Kingdom), Ligatures: None

Formatted: Font: (Default) Times New Roman, Font color: Black, English (United Kingdom), Ligatures: None

particles. The sample air is drawn into the ACSM through a ½-inch stainless steel tube at a flow rate of 3 L/min using an isokinetic sampling line. The particles are then focused by aerodynamic lenses before impacting on the vaporizer, heated at ~ 620 °C to generate gas-phase molecules that are then ionized by the filament. The ionized particles are then detected by the quadrupole mass spectrometer with unit mass resolution.

As described by Ng et al. (Ng *et al.*, 2011), aerosol mass concentrations are calculated from the difference between the sample mode and filter mode of the instrument, with each scan comprising 28 filter samples and 28 ambient samples, scanning over 32 seconds each to generate 30-minute time resolution data for our analysis.

The instrument's aerodynamic lens was aligned, and the flow calibration was performed before starting the data collection in April 2023. Similarly, the relative ionization efficiency (RIE) calibration (Ng *et al.*, 2011) was conducted at the beginning of the data collection period, during sampling, and again after 12 months of sampling, which covers the data duration. Time-dependent RIE values and ammonium nitrate (NH₄NO₃) response factors (RF) were applied to their respective sampling period. During all RIE calibrations, the response factor and RIE for both NO₃ and SO₄ remained stable within a 10% variation across the four calibrations conducted during the campaign.

Ambient black carbon (BC) mass concentration was measured using a seven-wavelength (370nm, 470nm, 520nm, 590nm, 660nm, 880nm, and 950 nm) aethalometer (model AE33, which shared the same sampling line as the ACSM). The reported total BC concentration values were determined based on light absorption via edlight absorption at 880 nm, with a Magee AE33 aethalometer

The AE33 automatically corrects for filter loading effects using a dual-spot sample collection method; hence, the filter loading effect compensation was not applied (Magee Scientific, 2017). BC source apportionment to distinguish BC from biomass burning and BC from fossil fuel burning was performed using the method described by Sandradewi et al (Sandradewi *et al.*, 2008). This approach assumes that the total optical absorption at 950 nm and 470 nm is the sum of biomass burning and fossil fuel burning fractions.

PM_{2.5} mass concentrations were obtained from a Teledyne T640 PM_{2.5} mass monitor (Teledyne, 2016) installed at the U.S. embassy in Kigali. The embassy is located approximately 10.6 km from the University

Formatted: Font: (Default) Times New Roman, Font color: Black, English (United Kingdom), Ligatures: None

Formatted: Font: (Default) Times New Roman, Font color: Black, English (United Kingdom), Ligatures: None

Formatted: Font: (Default) Times New Roman, Font color: Black, English (United Kingdom), Ligatures: None

Formatted: Font: (Default) Times New Roman, Font color: Black, English (United Kingdom), Ligatures: None

Formatted: Font: (Default) Times New Roman, Font color: Black, English (United Kingdom), Ligatures: None

Formatted: Font: (Default) Times New Roman, Font color: Black, English (United Kingdom), Ligatures: None

Formatted: Font: (Default) Times New Roman, Font color: Black, English (United Kingdom), Ligatures: None

Formatted: Font: (Default) Times New Roman, Font color: Black, English (United Kingdom), Ligatures: None

Formatted: Font: (Default) Times New Roman, Font color: Black, English (United Kingdom), Ligatures: None

Formatted: Font: (Default) Times New Roman, Font color: Black, English (United Kingdom), Ligatures: None

Formatted: Font: (Default) Times New Roman, Font color: Black, English (United Kingdom), Ligatures: None

Formatted: Font: (Default) Times New Roman, Font color: Black, English (United Kingdom), Ligatures: None

Formatted: Font: (Default) Times New Roman, Font color: Black, English (United Kingdom), Ligatures: None

Formatted: Font: (Default) Times New Roman, Font color: Black, English (United Kingdom), Ligatures: None

Formatted: Font: (Default) Times New Roman, Font color: Black, English (United Kingdom), Ligatures: None

Formatted: Font: (Default) Times New Roman, Font color: Black, English (United Kingdom), Ligatures: None

Formatted: Font: (Default) Times New Roman, Font color: Black, English (United Kingdom), Ligatures: None

Formatted: Font: (Default) Times New Roman, Font color: Black, English (United Kingdom), Ligatures: None

Formatted: Font: (Default) Times New Roman, Font color: Black, English (United Kingdom), Ligatures: None

Formatted: Font: (Default) Times New Roman, Font color: Black, English (United Kingdom), Ligatures: None

Formatted: Font: (Default) Times New Roman, Font color: Black, English (United Kingdom), Ligatures: None

Formatted: Font: (Default) Times New Roman, Font color: Black, English (United Kingdom), Ligatures: None

Formatted: Font: (Default) Times New Roman, Font color: Black, English (United Kingdom), Ligatures: None

of Rwanda sampling site. Temperature, relative humidity, wind speed, wind direction, and rainfall data were obtained from a nearby automatic meteorological station owned by [Meteo Rwanda](#) located at -1.955793 latitude and 30.05641 longitude for the same period of time.

Formatted: Font: (Default) Times New Roman, Font color: Black, English (United Kingdom), Ligatures: None

165 2.3 Data analysis

ACSM data were processed offline using ACSM local v1.6.2.1 in Igor Pro (Oregon USA WaveMetrics, 2024). Given that the instrument is equipped with a standard vaporizer, the particle Collection Efficiency (CE) was adjusted to 0.5, as recommended in the literature (Ng *et al.*, 2011). The CE accounts for particle loss associated with shape-related collection losses at the vaporizer due to the inefficient focusing of non-spherical particles, particle losses resulting from bounce effects of larger particles in the ionization region, and aerodynamic inlet losses as a function of particle diameter (Huffman *et al.*, 2005; Liu *et al.*, 2007; Matthew, Middlebrook and Onasch, 2008; Ng *et al.*, 2011). The RIE values for NH₄ and SO₄, along with the Response Factor (RF) for NO₃, were automatically loaded into the instrument's data acquisition software and applied to the raw data after each calibration. These factors were also used during post-processing to ensure that the correction factors were consistently applied, ensuring accuracy in the final data analysis.

Formatted: Font: (Default) Times New Roman, Font color: Black, English (United Kingdom), Ligatures: None

Formatted: Font: (Default) Times New Roman, Font color: Black, English (United Kingdom), Ligatures: None

Formatted: Font: (Default) Times New Roman, Font color: Black, English (United Kingdom), Ligatures: None

To ensure the quality of the calibration and instrument performance, the total NR-PM₁ was compared to the PM_{2.5} data obtained from the USA embassy T-640 (see Figure S3 in the supplemental information).

Formatted: Font: (Default) Times New Roman, Font color: Black, English (United Kingdom), Ligatures: None

Positive matrix factorization (Paatero and Tapper, 1994) and the PMF evaluation tool (PET v.3.06) were used to perform the source apportionment of the organic-only aerosol for the whole dataset. The PMF-derived source profiles were systematically selected based on the approach explained by Zhang *et al.* (Zhang *et al.*, 2011).

Formatted: Font: (Default) Times New Roman, Font color: Black, English (United Kingdom), Ligatures: None

Formatted: Font: (Default) Times New Roman, Font color: Black, English (United Kingdom), Ligatures: None

Formatted: Font: (Default) Times New Roman, Font color: Black, English (United Kingdom), Ligatures: None

Formatted: Font: (Default) Times New Roman, Font color: Black, English (United Kingdom), Ligatures: None

Formatted: Font: (Default) Times New Roman, Font color: Black, English (United Kingdom), Ligatures: None

3. Results and Discussion

3.1 NR-PM₁, BC, and PM_{2.5} mass concentration, chemical composition, and seasonal variation

185 Figure 1 shows the temporal variations in weekly mean concentrations of PM₁ components, including organic aerosols (Org), nitrate (NO₃), sulfate (SO₄), ammonium (NH₄), chloride (Cl), and black carbon

Formatted: Font: (Default) Times New Roman, Bold, English (United Kingdom), Subscript, Ligatures: None

Formatted: Font: (Default) Times New Roman, Bold, English (United Kingdom), Subscript, Ligatures: None

Formatted: Font: (Default) Times New Roman, Font color: Black, English (United Kingdom), Ligatures: None

Formatted: Font: (Default) Times New Roman, Font color: Black, English (United Kingdom), Ligatures: None

(BC). There is a clear seasonal variation in both speciated PM₁ (NR-PM₁+ BC) and PM_{2.5} concentrations, with higher concentrations during the dry seasons (mean, for both JJA and DJF, PM₁ = 37 ± 11 μg m⁻³) than the rainy seasons (mean, for both MAM and SON, PM₁ = 28 ± 6 μg m⁻³; Fig. S4). In Kigali, at the urban background site, the annual mean PM₁ was 31 ± 15 μg m⁻³ with an annual mean BC concentration of 4.5 ± 3 μg/m³. Similarly, at the U.S. Embassy in Kigali, urban roadside site (PM_{2.5} UE in Figure 1), the annual mean PM_{2.5} concentration was 41 ± 23 μg m⁻³. ~~with a seasonal mean concentration of 5.9 μg/m³ in the dry seasons and 3.8 μg/m³ in the rainy seasons.~~

Concurrent measurements of speciated PM₁ and PM_{2.5} in urban Kigali showed a strong correlation (R² = 0.91) with a -slope of 0.65 (See Figure S3 in supporting information). Some of the mass differences between speciated PM₁ and PM_{2.5} can likely be attributed to the impact of dust, which cannot be detected by the ACSM. In addition, site characteristics may play a role, as the US embassy site is classified as an urban near-road site compared to the UR/CST site, classified as an urban background site. The annual mean concentration of PM_{2.5} of 41 μg m⁻³ is comparable with the mean PM_{2.5} concentration of 42.6 μg m⁻³ reported by Gahungu et al. in the same city (Gahungu and Kubwimana 2022b). However, it was higher than the daily mean concentration of PM_{2.5} of 25 μg m⁻³ reported by Kalisa et al. for a 3-month data span in both dry and rainy-wet seasons (Kalisa et al., 2018) and comparatively higher than the nighttime filter-based measurements at the Rwanda Climate Observatory (Dewitt et al., 2019; Andersson et al., 2020; Kirago et al., 2022).

Organic aerosols (OA) dominate the PM₁ composition, accounting for 73% of the total mass loading, followed by black carbon (BC) at 16%. Inorganic species collectively contributed 11% of the total PM₁, distributed as follows: NO₃ at 6%, SO₄ at 2%, NH₄ at 2%, and Cl at 1%. The compositions are similar to the findings from a remote area in the same country by Kirago et al. 2022 (Kirago et al., 2022) (mean of all seasons: OM at 72%, BC at 4.5%, SO₄ at 12.6%, NO₃ at 4%, and NH₄ at 5.2%). However, the SO₄ and NH₄ fractions were 2.6 was 6 times lower, and the BC fraction was 43.5 times higher at this urban site compared to the remote site.

The high contribution of OA to PM₁ mass was also recorded in previous studies in African cities. For example, aircraft measurements in South Africa showed that OA contributed 53% of PM₁ mass, though

Formatted: Font: (Default) Times New Roman, Font color: Black, English (United Kingdom), Ligatures: None

Formatted: Font: (Default) Times New Roman, Font color: Black, English (United Kingdom), Ligatures: None

Formatted: Font: (Default) Times New Roman, Font color: Black, English (United Kingdom), Ligatures: None

Formatted: Font: (Default) Times New Roman, Font color: Black, English (United Kingdom), Ligatures: None

Formatted: Font: (Default) Times New Roman, Font color: Black, English (United Kingdom), Ligatures: None

Formatted: Font: (Default) Times New Roman, Font color: Black, English (United Kingdom), Ligatures: None

Formatted: Font: (Default) Times New Roman, Font color: Black, English (United Kingdom), Ligatures: None

Formatted: Font: (Default) Times New Roman, Font color: Red, English (United Kingdom), Ligatures: None

Formatted: Font: (Default) Times New Roman, Font color: Black, English (United Kingdom), Ligatures: None

Formatted: Font: (Default) Times New Roman, Font color: Black, English (United Kingdom), Ligatures: None

Formatted: Font: (Default) Times New Roman, Font color: Black, English (United Kingdom), Ligatures: None

Formatted: Font: (Default) Times New Roman, English (United Kingdom), Ligatures: None

Formatted: Font: (Default) Times New Roman, English (United Kingdom), Ligatures: None

Formatted: Font: (Default) Times New Roman, English (United Kingdom), Ligatures: None

Formatted: Font: (Default) Times New Roman, Font color: Black, English (United Kingdom), Ligatures: None

Formatted: Font: (Default) Times New Roman, Font color: Black, English (United Kingdom), Ligatures: None

Formatted: Font: (Default) Times New Roman, Font color: Black, English (United Kingdom), Ligatures: None

Formatted: Font: (Default) Times New Roman, Font color: Black, English (United Kingdom), Ligatures: None

Formatted: Font: (Default) Times New Roman, Font color: Black, English (United Kingdom), Ligatures: None

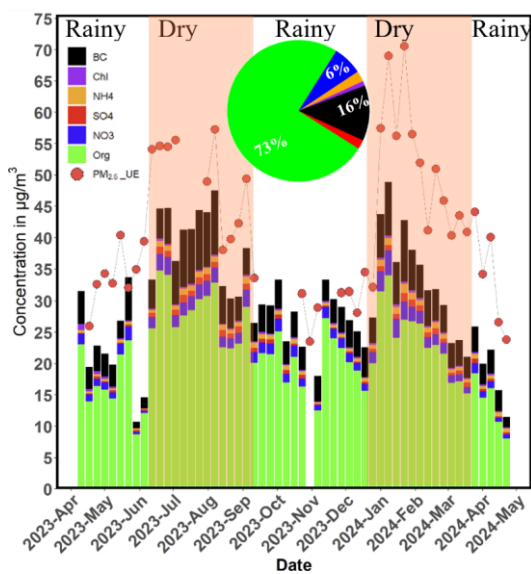
Formatted: Font: (Default) Times New Roman, Font color: Black, English (United Kingdom), Ligatures: None

Formatted: Justified, Space After: 0 pt, Line spacing: 1.0 lines, Don't adjust space between Latin and Asian text

215 there was a larger contribution of sulfate (27%)(Brito *et al.*, 2018). Additionally, filter-based
measurements in Dar es Salaam, Tanzania, showed that OA accounted for 68% and inorganic species
accounted for 24% of PM₁ mass (Mkoma *et al.*, 2009).

220 OA dominates the PM₁ composition across both rainy and dry seasons with a relatively stable fractional
contribution: 74% on average during the dry season (mean of JJA and DJF) and 71% during the rainy
season (mean of MAM and SON) (see Figure 4). A similar seasonal composition was also recorded at a
remote site in the same country, with 72% and 69% as the mean of the dry and rainy seasons, respectively
(Kirago *et al.*, 2022).

Field Code Changed



225 Figure 1: Measured PM₁ and PM_{2.5} in Kigali, Rwanda. Each stacked bar represents the weekly mean
concentrations of NR-PM₁ components (SO₄, Org, NO₃, NH₄, Chl) and Black Carbon (BC). Red dots
indicate PM_{2.5} concentrations measured at the U.S. Embassy, located about ~~640~~ km from the ACSM
sampling site. The pie chart depicts the overall mean fractional contribution of the total PM₁ mass loading
(NR-PM₁ + BC). The shaded areas highlight the dry seasons in Rwanda, providing context for seasonal
variations in particulate matter.

230

3.2 Diurnal variations in PM₁ mass and composition

The ~~seasonal campaign~~ average diurnal variation in PM₁ components (NR-PM₁ and BC) is presented in Figure ~~-22~~; and the annual average diurnal ~~plot seasonal diurnal~~ patterns are shown in Figure S4 in the supporting information. In all four seasons, the diurnal patterns show the interplay of emissions and atmospheric processes on pollutant concentrations. These include traffic emissions from busy roads near the sampling site, with 85% of vehicles in Kigali being over 20 years old (Niyibizi *et al.*, 2015; MINEFRA, 2018a; UN Environment, 2019; NIS Rwanda, 2021). Additionally, emissions from solid fuels contribute significantly, as biomass energy accounts for approximately 85% of the total energy used for cooking in Kigali (MINEFRA, 2015, 2018b; UN Environment, 2019), including emissions from restaurants in the downtown area and densely populated residential areas near the station. Diurnal variability is also influenced by meteorology, including changes in the planetary boundary layer height (PBLH) that is expected to be shallower during night and morning time (6:00 pm to 7:00 am) and expand during the daytime, and hence controls the particle mixing volume and concentration (Nyeki *et al.*, 1998; Engeln and Teixeira, 2013).

OA, BC, and NO₃ all exhibit an early morning peak (6:00 am to 9:00 am), a midday decrease, and a second evening peak (6:00 pm to 10:00 pm). The morning peak coincides with increased anthropogenic activities, likely associated with rush hour traffic and cooking activities in the morning. The midday dips in particle concentrations can be attributed to enhanced atmospheric mixing and reduced anthropogenic activities. Daytime increases in the planetary boundary layer height increase the mixing volume and hence reduce the particle concentration during the daytime (Subramanian *et al.*, 2020). Additionally, higher wind speeds during the daytime contribute to particle dilution (Figures 2 and Figure S2(b) in the Supporting Information). The evening peak is likely due to a combination of decreasing boundary layer height (von Engeln and Teixeira, 2013) after sunset (typically around 6 pm) and the evening rush hour.

The overall intra-day variations in concentrations of OA, BC, and NO₃ are large. Annually averaged, OA concentrations are ~20 – 25 µg m⁻³ from midnight to 10 am but fall to ~12 µg m⁻³ in mid-afternoon. Similarly, BC concentrations change from ~7 µg m⁻³ to ~2.5 µg m⁻³ over the same period (see Figure S4). Across all seasons, organic components dominate PM₁, with their proportion peaking during the long dry season (75% of total PM₁) and being slightly lower during the short rainy season (73% of total PM₁).

Formatted: Subscript

Formatted: Font: (Default) Times New Roman, English (United States), Ligatures: None

Formatted: Not Highlight

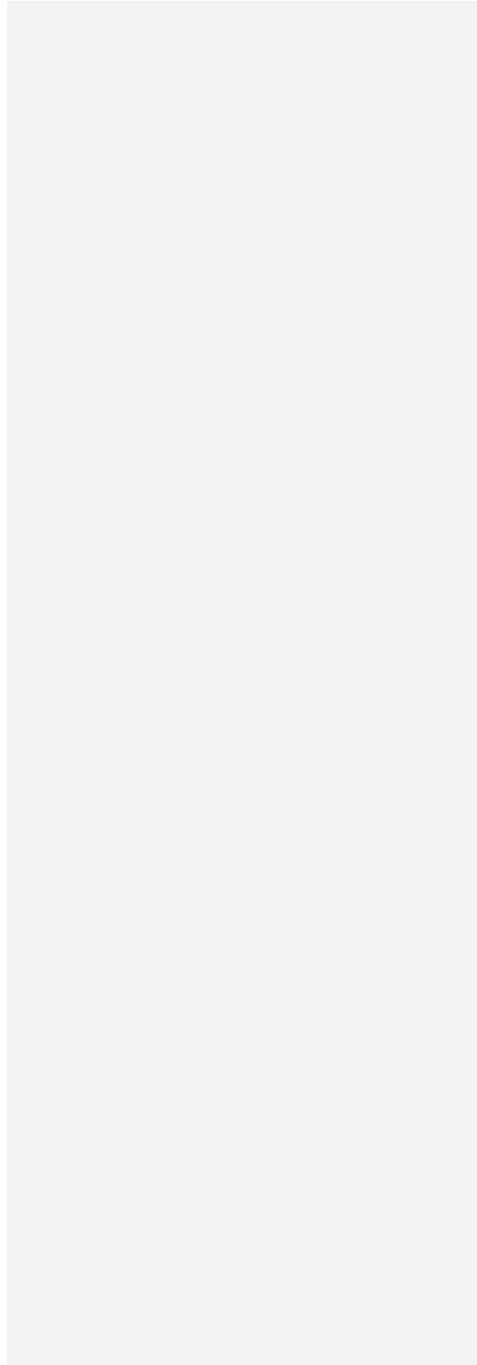
Black Carbon (BC) is the second-largest component, with its contribution ranging between 15% and 22%.

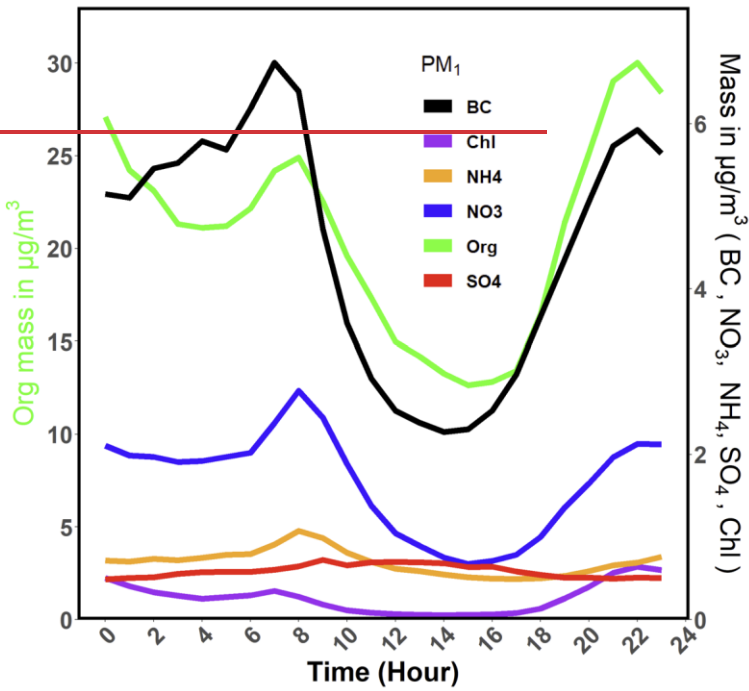
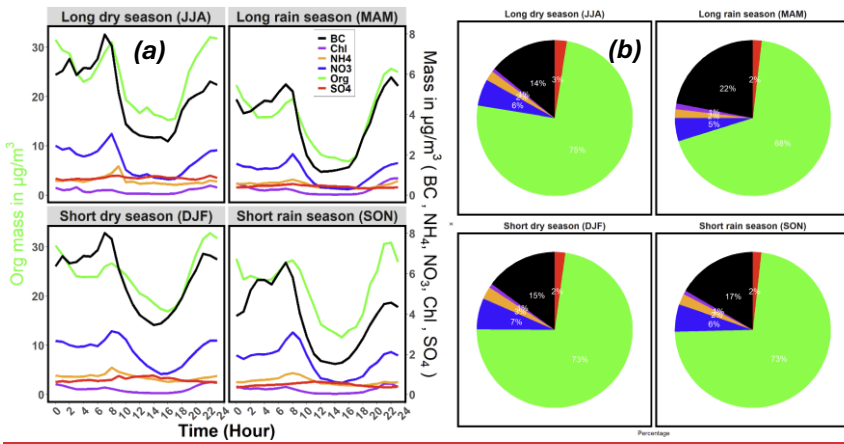
260 The highest BC composition was observed during the long rainy season, showing a similar trend to
Abidjan, Côte d'Ivoire (Anand et al., 2024). The diurnal patterns during the dry seasons (DJF) show a
higher magnitude on an hourly basis compared to those in the rainy season. However, SO₄ remained
relatively constant across all four seasons. The JJA season exhibits the highest morning and evening
peaks, reflecting the influence of morning rush hour emissions, a shallower planetary boundary layer
265 height, and the absence of major PM removal processes such as precipitation scavenging.

The shape of the diurnal patterns offers insight into potential emission sources and aerosol processing. The morning peak in BC occurs at 7:00 am. This is one hour earlier than the corresponding morning peak in both OA and NO₃. There are a few possible reasons for the earlier peak in BC. One is that the anthropogenic source mix changes throughout the morning, with the relative impacts of cooking and traffic changing over the period from ~6:00–10:00 am. A second possibility is that the slight delay in the OA and NO₃ peaks reflects the importance of secondary OA and nitrate formation, and the one-hour delay in their peaks relative to BC is the result of the time needed for chemical conversion from precursor gases to PM components.

275 OA, BC, and NO₃ all have contributions from local emissions and, therefore, exhibit strong intra-day patterns associated with anthropogenic activities. SO₄, on the other hand, has a much flatter diurnal profile. There is no morning increase in sulfate, though there is a slight midday increase from 10 am to 6 pm. This suggests that SO₄ concentrations in Kigali are regional, reflecting the lack of local SO₄ emissions or SO₂ sources that would contribute to daytime SO₄ formation. For example, there are no coal-fired power plants in Rwanda or the nearby areas of neighbouring countries. (Monitor, 2025). Back trajectory analysis (Figure S12) showed that the emissions from the active stratovolcano Nyiragongo, which erupted in June 2021 and is located at 1.52°S latitude and 29.25°E longitude in the Democratic Republic of Congo (DRC), do not move toward Kigali (Smithsonian Institute, 2025).

|





290

Figure 2: Seasonal (JJA, SON, DJF, and MAM) diurnal profiles of NR-PM₁ components (Chl, NH₄⁺, NO₃⁻, SO₄²⁻, Org), and BC (Figure a). Organic aerosol (Org) concentrations are shown on the left y-axis, while all inorganic species are plotted on the right y-axis. Figure (b) shows the season PM₁ compositions

295

Campaign average diurnal profile of NR-PM₁ composition (Chl, NH₄, NO₃, SO₄, Org, and BC) with OA plotted on the left y-axis and the

3.3 Average mass spectrum and contribution of tracer ions

Figure S7 in the Supporting Information shows the campaign-average mass spectrum (MS) measured by the ACSM. The most abundant ions in the mass spectrum are *m/z* 18 (H₂O⁺) and 44 (CO₂⁺). *M/z* 44 is commonly used as a tracer for aged OA (Ng *et al.*, 2011). It accounts for 10.5% of the measured organic aerosol mass, whereas *m/z* 18 is for particle water contents.

300

Other prominent tracer ions in the mass spectrum include *m/z* 43, which has contributions from both C₃H₇⁺, associated with fresh emissions, and C₂H₃O⁺, linked to secondary organic aerosol. *M/z* 43 contributed 7% of the OA mass in Kigali. Additional tracer ions, such as tracers for urban fresh traffic emissions (e.g., *m/z* 57 (C₄H₉⁺)) and fresh biomass burning emissions (*m/z* 60, (C₂H₄O₂⁺)) (Ng *et al.*, 2011), together contribute approximately 3.5% of the average PM₁ mass loading.

305

Inorganic species also contribute significantly to PM₁, with notable nitrate peaks at *m/z* 30 and *m/z* 46, sulfate at *m/z* 48 and *m/z* 64, and ammonium at *m/z* 16 and *m/z* 17. Small peaks at *m/z* 35 and *m/z* 36 indicate that chloride makes a minimal contribution (see Figure S7 in the supporting information).

310

NO₃ accounts for 6% of the total PM₁ mass and consists of both organic and inorganic nitrate species. The ratio of *m/z* 46 to *m/z* 30 is often used to quantify the relative amounts of inorganic and organic nitrate using equation 1 (Lanz *et al.*, 2007; Ng *et al.*, 2011; Budisulistiorini *et al.*, 2013).

$$f_{OrgNO_3} = \frac{(R_{ambient} - R_{NH_4NO_3})(1 + R_{OrgNO_3})}{(R_{OrgNO_3} - R_{NH_4NO_3})(1 + R_{ambient})} \quad (1)$$

Formatted: Font: (Default) Times New Roman, English (United Kingdom), Ligatures: None

Formatted: Font: (Default) Times New Roman, English (United Kingdom), Ligatures: None

Formatted: Font: (Default) Times New Roman, English (United Kingdom), Ligatures: None

Formatted: Font: (Default) Times New Roman, English (United Kingdom), Ligatures: None

Formatted: Font: (Default) Times New Roman, English (United Kingdom), Ligatures: None

Formatted: Font: (Default) Times New Roman, English (United Kingdom), Ligatures: None

Formatted: Font: (Default) Times New Roman, English (United Kingdom), Ligatures: None

Formatted: Font color: Black, Kern at 16 pt

Formatted: Level 1, Space Before: 30 pt, After: 18 pt

Formatted: Font: (Default) Times New Roman, Ligatures: None

Formatted: Font: (Default) Times New Roman, Ligatures: None

Formatted: Font: (Default) Times New Roman, English (United States), Ligatures: None

315

Here, f_{OrgNO_3} is the mass fraction of the total ACSM nitrate that is organic, R is the ratio of m/z 46 to m/z 30, R_{ambient} is a calculated ratio using time series ambient data, $R_{\text{NH}_4\text{NO}_3}$ is calculated ratio using periodic instrument relative ionization efficiency (RIE) calibration data, whereas R_{OrgNO_3} can be determined from atomizing laboratory standards of organic nitrates or from literature values. For example, Brito et al. (Brito *et al.*, 2018) used $R_{\text{OrgNO}_3} = 0.1$. An alternative approach, proposed by Day et al (Day *et al.*, 2022), uses a ratio-of-ratios method. This method amends equation 1 using $R_{\text{NH}_4\text{NO}_3}/R_{\text{OrgNO}_3}$. The advantage of the ratio-of-ratios R_{ambient} approach is that it accounts for instrument-to-instrument variations in both $R_{\text{NH}_4\text{NO}_3}$ and R_{OrgNO_3} , instead relying on a constant ratio of ratios for most organic nitrates ($R_{\text{NH}_4\text{NO}_3}/R_{\text{OrgNO}_3} = 2.75$). Additionally, Werden et al (2023) presented a method for determining f_{OrgNO_3} using R_{ambient} (Werden *et al.*, 2023), as shown in SI Section II.

Using the above ratio method, the calculated ratios were 0.25 ± 0.6 , 0.56 ± 0.2 , and 0.12 ± 0.06 (similar to the literature value) for R_{ambient} , $R_{\text{NH}_4\text{NO}_3}$ and R_{OrgNO_3} respectively. With hourly values ranging from 0.02 to 1.11. Figure S5 in the supporting information shows the results of calculating f_{OrgNO_3} using the above three approaches (literature $R_{\text{OrgNO}_3} = 0.1$, ratio-of-ratios and calculated R_{ambient} and Ratio-of-ratios method of Werden et al.). All three approaches indicate that organic nitrates make up a significant fraction of the observed nitrate. The ambient ratio method attributes the particle organic nitrate as $\sim 61\%$ of the total organic nitrate, assuming with $R_{\text{OrgNO}_3} = 0.1$ yields the an organic nitrate fraction of $\sim 70\%$, whereas and the ratio-of-ratios approach yields f_{OrgNO_3} near 100%. Therefore, both approaches indicate that organic nitrates make up a significant fraction of the observed nitrate. The presence of a slight peak in NH_4 during the morning rush hour (Figure 2) suggests that at least a portion of the nitrate is inorganic, and therefore, the f_{OrgNO_3} from the ratio-of-ratios approach might be an overestimation.

The annual average diurnal profile of four OA tracer ions (m/z 43, 44, 57, and 60) is shown in Figure 3. The mass concentrations of all four tracer ions show a similar diurnal pattern as the total OA mass (shown in Figures 2 and S4): there is a morning increase in concentration, followed by an afternoon minimum, and concentrations rise again in the evening. While all four of these ions show the same general pattern,

Formatted: Font: (Default) Times New Roman, Ligatures: None

Formatted: Font: (Default) Times New Roman, Ligatures: None

Formatted: Not Highlight

Formatted: Not Highlight

the slight differences in their behavior provide insights into PM sources and chemical processing in Kigali.

345 *M/z* 60 is a tracer for biomass burning emissions. The morning maximum concentration occurs from 6-7 am and is 1.5 times higher than the minimum concentration observed from 2-4 am. Many people in Kigali (85%) use biomass fuel for cooking (MINEFRA, 2015). This morning's increase in *m/z* 60 is likely from cooking activities before the start of the workday.

M/z 57 is commonly used as a tracer for fresh fossil fuel combustion emissions, especially from traffic.

350 The morning peak in *m/z* 57 mass concentration ($0.6 \mu\text{g}/\text{m}^3$) occurs at 7:00 am, with slightly lower concentrations at 8:00 am. This mirrors the diurnal pattern of BC (Fig. 2), which also has a morning maximum at 7 am (~~annual mean: 6.8 $\mu\text{g}/\text{m}^3$~~ see Figure S4). The high concentrations of both BC and *m/z* 57 suggest that the morning rush hour is most intense from 7-8 am. The morning peaks in BC and *m/z* 57 occur slightly after the morning peak in *m/z* 60 ($0.3 \mu\text{g}/\text{m}^3$); this suggests that while both cooking and traffic are important sources in the morning hours, cooking activity starts slightly before traffic volume increases.

M/z 44 is a tracer for oxygenated secondary organic aerosol (SOA). *M/z* 44 also has a morning peak. The morning peak in *m/z* 44 ($2.3 \mu\text{g}/\text{m}^3$) occurs at 8:00-9:00 am, after the earlier morning peaks in *m/z* 60 and *m/z* 57. This is suggestive that the morning increase in *m/z* 44 is due to the rapid formation of SOA and

360 that the vehicle and biomass-burning emissions associated with anthropogenic activities are important sources of SOA precursors. Traffic emissions are a well-known source of SOA precursor (Drew R. Gentner, 2016). This is especially true for older vehicles, poorly maintained, or otherwise higher-emitting than new vehicles with modern emission control systems (Sitati et al., 2022).

M/z 43 is a marker for both primary emissions (C_3H_7^+) and SOA ($\text{C}_2\text{H}_3\text{O}^+$). Our quadrupole ACSM has unit mass resolution and, therefore, cannot separate these isobaric ions. The diurnal pattern of *m/z* 43 reflects its dual nature as a marker of primary and secondary OA in Q-ACM. The concentration of *m/z* 43 rises rapidly from 6-7 am, coincident with the morning increase in the concentration of *m/z* 57. This initial increase in *m/z* 43 concentration is likely associated with fresh vehicle emissions. There is a further increase in *m/z* 43 concentration from 8-9 am, coincident with the rapid increase in *m/z* 44 concentration.

Formatted: Not Highlight

Formatted: Not Highlight

Formatted: Not Highlight

Formatted: Not Highlight

Formatted: Not Highlight

370 This further increase in m/z 43 is likely due to SOA formation from vehicles and biomass burning emissions.

The temporal patterns of the four marker ions shown in Figure 3 provide insight into sources and atmospheric processes. They all decrease during the afternoon. As with the PM components shown in Figure 2, this decrease is likely due to a combination of changing anthropogenic emissions (e.g., less traffic outside of the morning rush hour), increasing boundary layer height, and faster winds. Concentration rises again in the evening due to a combination of a sinking boundary layer after sunset and evening traffic and cooking activities.

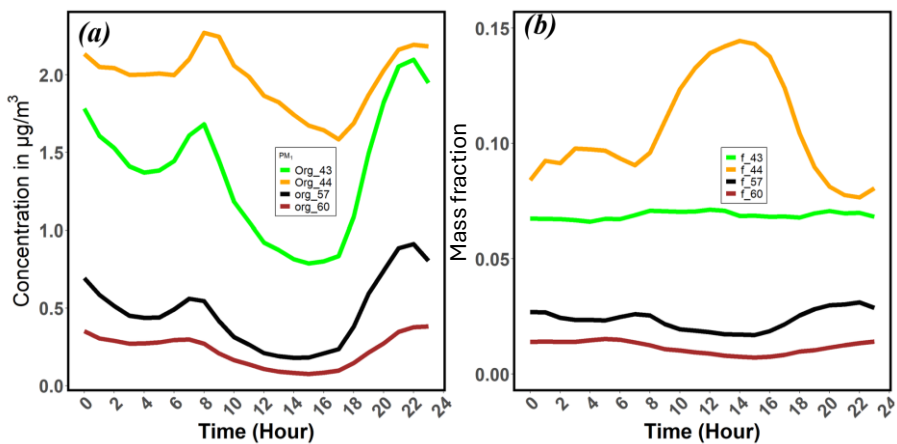
While concentrations of all four tracer ions decrease during the day, the decrease in m/z 44 is much smaller than for the other ions. For example, the ratio of the morning peak (7:00 am) to the afternoon trough (2:00 pm) in m/z 57 is ~ 3.3 , and the ratio in m/z 44 concentration (8:00 am versus 4:00 pm) is ~ 1.3 . This is likely due to the sustained formation of SOA throughout the day. Days in Kigali are consistently sunny (Figure S2 in the Supporting Information), and there is likely a large pool of reactive organic gases available to form SOA. Thus, the impact of boundary-layer driven dilution is larger for ions associated purely with primary emissions (e.g., m/z 57) than for ions associated with SOA.

385 Concentrations of m/z 43, 57, and 60 are all higher in the evening hours ($\sim 8:00$ - $11:00$ pm) than during the morning rush hour. The pattern of traffic and cooking emissions is also reversed in the evening compared to the morning. The late-day increase in the concentrations of m/z 57 and 43 precedes the increase in m/z 60. This is consistent with expected activity patterns, as people travel home from work before cooking at night.

390 The mass fractions of each tracer ion, shown in Figure 3b, offer additional insight into the competition between emissions, chemistry, and dilution. The diurnal variation of the mass fraction of m/z 57 in OA (f_{57}) is similar to the trend in m/z 57 mass. There are morning and evening peaks, with a slightly higher peak in the evening and a midday trough. The ratio of the peaks to the trough is smaller for f_{57} than for m/z 57 mass (1.5 and 3.3 for f_{57} and m/z 57, respectively). This reflects the large role that boundary layer dilution plays on mass concentrations and suggests that traffic activity, and hence emissions, remain high throughout the day.

The diurnal pattern in f_{44} shows a different trend. It rapidly increases after 7 am and peaks at $f_{44} = 0.14$ at 2:00 pm. The diurnal trend in f_{44} thus indicates that there is rapid formation of SOA, especially in the hours immediately following the high emissions associated with the morning rush hour. After 2 pm, f_{44} gradually decreases as solar intensity diminishes until sunset at 6:00 pm. Taken together, Figs 3a and 3b suggest that there is strong and sustained SOA production throughout the day and that SOA production is fast enough to at least partly counteract the large and rapid boundary layer-driven dilution that occurs during midday.

The diurnal profile of the normalized contribution of m/z 43 (f_{43}) remains relatively flat throughout the day. This is a result of the combined role of m/z 43 as an indicator for primary and secondary OA. $C_3H_7^+$ is emitted during the morning rush hour, and its concentration decreases with the expansion of the boundary layer and oxidation chemistry. $C_2H_5O^+$ increases due to SOA formation through photochemistry. These opposing behaviors result in a relatively constant f_{43} throughout the day.



410 Figure 3: Diurnal patterns of individual tracer ions: (a) absolute mass concentrations and (b) mass fractions.

Formatted: Not Highlight

3.4 PM Source Apportionment

We performed PMF source apportionment of the OA-only PM₁ masses using PMF2.exe and PMF Evaluation Tool version 3.08. The number of factors and source profiles were systematically selected and validated following the recommendations of Ulbrich et al. (Ulbrich *et al.*, 2009). The most interpretable solutions were chosen based on Q/Q_{Expected} (Q : sum of squared scaled residuals), changes in the total sum of squared scaled residuals with an increasing number of factors, normalized fractional contributions of individual source profiles, and factor spectra comparisons with standard AMS mass spectra (Zhang *et al.*, 2011). Section IV of the Supporting Information shows more details on the PMF analysis, including a comparison of three versus four-factor solutions.

Figure 4 (a) shows the mass spectral profiles of deconvolved organic-only PM₁ source apportionment using PMF. Three factors, Oxygenated Organic Aerosol (OOA), Hydrocarbon-like Organic Aerosol (HOA), and Biomass-Burning Organic Aerosol (BBOA) were identified (Figure 4). The mass spectrum of HOA is characterized by the pronounced hydrocarbon ion series of C_nH_{2n+1} and C_nH_{2n-1}, consistent with primary emissions from traffic and fossil fuel combustion (Zhang *et al.*, 2011; He *et al.*, 2022). Important peaks in this mass spectrum include m/z 41, 43, 55, 57, 69, and 71. The HOA source profile has a high f_{57} (= 0.095), exhibiting a normalized signal fraction of 0.095, further supporting the assignment of this factor to primary hydrocarbon sources.

In the BBOA mass spectrum, the most prominent peak is at m/z 29 with an abundance $m(f_{29} = \text{ass fraction of } 0.17)$, likely indicating small oxygenated fragments associated with the incomplete combustion of biomass. Another significant peak is at m/z 60 ($f_{\text{fraction}60} = 0.035$), which is a widely recognized tracer for levoglucosan-like compounds, supporting the biomass burning origin. The peak at m/z 43 ($f_{43} = 0.08$), reflecting mixed hydrocarbon and oxygenated fragments.

The OOA mass spectrum is characterized by the large abundance of m/z 44 (with a mass fraction of $f_{44} = 0.24$), indicative of aged, highly oxidized organic material dominated by CO₂⁺ fragments. This ion is a well-established marker for secondary organic aerosol (SOA) formation (Matthew, Middlebrook and Onasch, 2008; Ng *et al.*, 2011; Zhang *et al.*, 2011).

Formatted: Not Highlight

Formatted: Not Highlight

Formatted: Font: (Default) Times New Roman, English (United Kingdom), Ligatures: None

Formatted: Font: English (United Kingdom), Ligatures: None

Formatted: Font: Not Italic, English (United Kingdom), Ligatures: None

Formatted: Font: English (United Kingdom), Ligatures: None

Formatted: Font: Not Italic, English (United Kingdom), Ligatures: None

Formatted: Font: English (United Kingdom), Ligatures: None

Formatted: Font: Italic

Formatted: Font: (Default) Times New Roman, English (United Kingdom), Ligatures: None

Formatted: Default Paragraph Font, Font: (Default) Times New Roman, English (United Kingdom), Ligatures: None

Formatted: Font: Italic

Formatted: Font: (Default) Times New Roman, English (United Kingdom), Subscript, Ligatures: None

Formatted: Font: (Default) Times New Roman, English (United Kingdom), Ligatures: None

Formatted: Font: Italic

Formatted: Font: (Default) Times New Roman, English (United Kingdom), Ligatures: None

Formatted: Font: (Default) Times New Roman, English (United Kingdom), Ligatures: None

Formatted: Font: (Default) Times New Roman, English (United Kingdom), Ligatures: None

Formatted: Font: (Default) Times New Roman, English (United Kingdom), Ligatures: None

Formatted: Default Paragraph Font, Font: (Default) Times New Roman, English (United Kingdom), Ligatures: None

Formatted: Subscript

Formatted: Font: (Default) Times New Roman, English (United Kingdom), Ligatures: None

Formatted: Font: (Default) Times New Roman, English (United Kingdom), Ligatures: None

Formatted: Font: Italic

Formatted: Font: (Default) Times New Roman, English (United Kingdom), Subscript, Ligatures: None

Formatted: Font: (Default) Times New Roman, English (United Kingdom), Ligatures: None

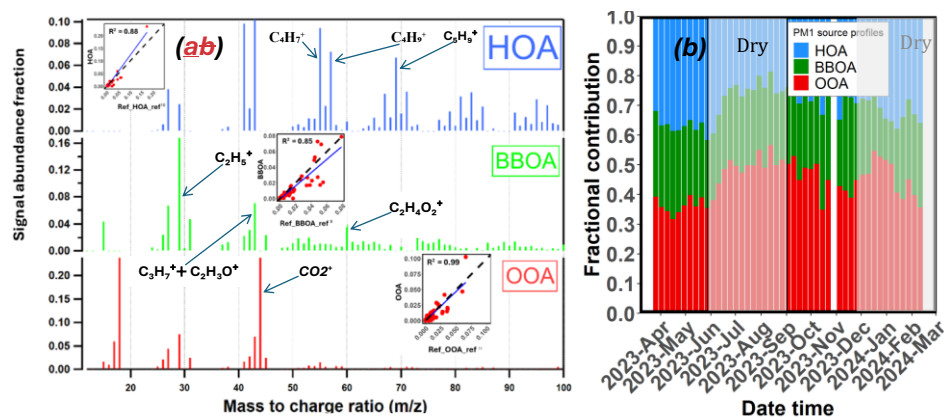
Formatted: Font: (Default) Times New Roman, English (United Kingdom), Ligatures: None

Formatted

440 The HOA, BBOA, and OOA factor profiles show strong similarity to published profiles from ambient
deconvolved spectra in other cities, indicating consistency with existing data. When compared to the
reference mass spectra (Ulbrich, I.M., 2025), all three factors exhibited strong correlations. The HOA
factor had an R^2 value of 0.88 and a ~~slope_slope~~ of 0.85, while the BBOA factor achieved an R^2 of 0.85
and a ~~slope_slope~~ of 0.94. Similarly, the OOA factor profile showed an exceptionally strong correlation
445 with the reference spectra, with an R^2 value of 0.99 (see Figure S10 in the supplementary information
document).

PMF results indicate that there are large contributions from both primary and secondary OA. Over the
course of the year, the mean contributions of each factor are 45% OOA, 32% HOA, and 23% BBOA.
Figure 4b further shows that there is little seasonal variation in source strengths. During the dry season,
450 the mean composition is 47% OOA, 23% BBOA, and 30% HOA, versus 41% OOA, 28% BBOA, and
31% HOA during the rainy wet season. This suggests that the changes in PM_{10} mass between the dry and
rainy seasons (Figure 1) are due more to changes in particle loss (e.g., via wet deposition) and chemical
production rather than shifts in primary emissions, chemical processing, or source strengths.

455



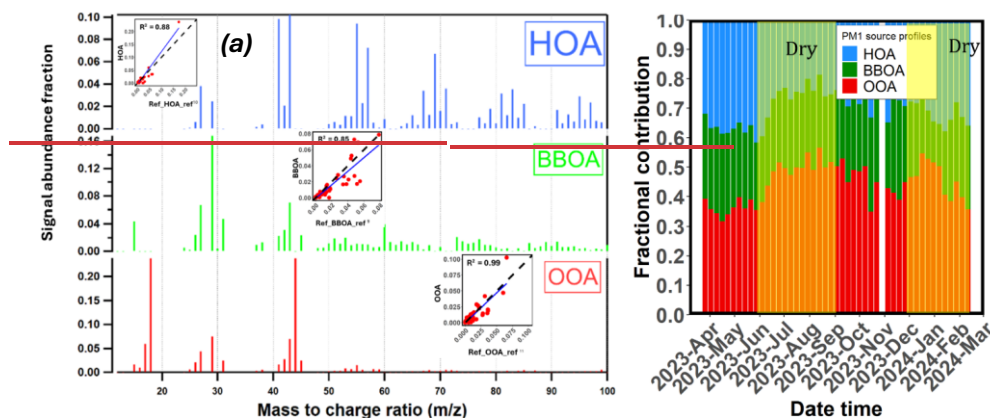
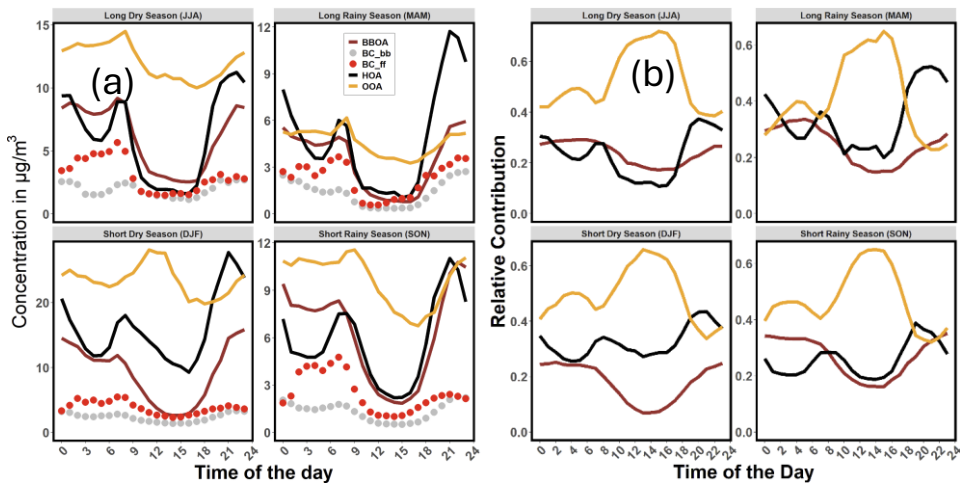


Figure 4: (a) PMF factor profiles for HOA, BBOA, and OOA. The inset scatter plots show the comparison of the PMF source profiles with reference source profiles, and (b) show the seasonal variations in source fractional contributions, with each bar representing the mean relative fractional contribution of the three sources for each week. The yellow shading indicates the two dry seasons.

The diurnal pattern of the source strengths is shown in Figure 5. As expected, they mirror the trends in tracer ions shown in Figure 3. The OOA factor peaked during the daytime, mirroring f_{44} , underscoring the important role of photochemistry and secondary organic aerosol production at the site. OOA concentrations are less impacted by dilution than HOA and BBOA due to strong daytime SOA production (production) (Figure 5 (a) panel and Figure S13).

Formatted: Subscript



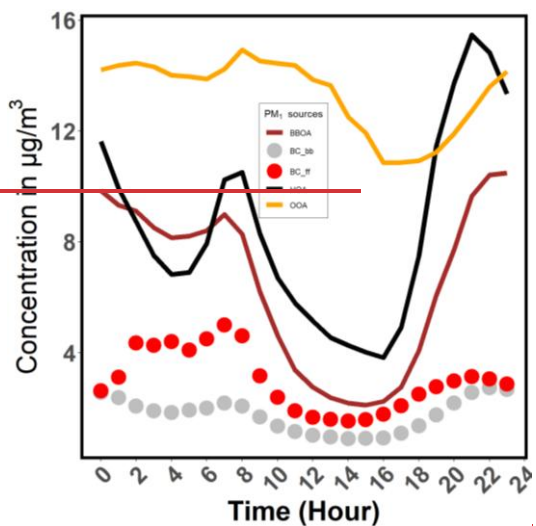


Figure 5: Seasonal diurnal patterns of PMF-resolved organic-only PM₁ sources and BC components (BC-ff and BC_bb), presented as absolute mass concentrations (a) and relative PMF source contributions (b).

Both BBOA and HOA factors show morning and evening peaks, which mirror anthropogenic activities (see Figure 5-(a)). The morning peak in BBOA occurs before the morning peak in HOA (except during the MAM season, when they are coincident), associated with rush hour traffic. In the afternoon, the trend is reversed, with HOA concentrations increasing and reaching an evening peak before BBOA. For both BBOA and HOA, the evening peak in concentrations is larger than the morning peak in all seasons. Throughout most of the day, concentrations of HOA are smaller than concentrations of OOA. However, during the evening peak from ~6:00-10:00 pm, HOA concentrations are larger than OOA concentrations.

Figure 5b shows the fractional contribution of each source factor to the total OA for each season. In all seasons, OOA is the most abundant factor at nearly all hours of the day. The OOA fraction rises dramatically during daylight hours from ~40% of OA mass overnight to >60% during the day, consistent with strong production of secondary OA. The fractional abundance of HOA shows strong diurnal peaks associated with the morning and evening rush hours.

The normalized source contribution for the PMF sources and BC components indicates that OOA (Figure 5 (b)) is the dominant organic PM source in all seasons, showing relatively stable contributions throughout the day, slightly increases during the short dry season (DJF), and is lower in the long rainy season (MAM). Potentially due to the transported aged aerosol originating from the wide-scale biomass burning in the northwest of Rwanda during the DJF (Dewitt *et al.*, 2019). BBOA shows strong diurnal peaks in the dry seasons (JJA and DJF), indicating enhanced biomass burning during morning and evening hours. BC_{bb} mirrors this pattern but with slightly lower contribution. BC_{ff}, linked to fossil fuel combustion, exhibits clear rush-hour peaks, particularly in DJF and MAM. HOA remains a minor but consistently present contributor, with slight morning elevations in DJF.

Formatted: Not Highlight

BC contributes ~16% of the PM₁ mass. Using the algorithm developed by Sandradewi *et al.* (Sandradewi *et al.*, 2008), BC was decomposed into BC from fossil fuel combustion (BC_{ff}) and BC from biomass burning (BC_{bb}) fractions. The annual mean BC measured in Kigali consists of 59% BC_{ff} and 41% BC_{bb}. Figure S6 in the supporting information shows that there is minimal seasonal variation in BC source apportionment. Across all seasons, BC_{ff} contributed 55–63% of the total BC mass loading, with BC_{bb} contributing 37–45% of the observed BC mass. These results are contrary to the BC composition recorded at the Rwanda Climate Observatory (RCO), which is located in a remote area. There, BC was 8–13% BC_{ff} and 87–92% BC_{bb} (Andersson *et al.*, 2020; Kirago *et al.*, 2022). This difference may be attributed to the site characteristics, where RCO is a remote site compared to the measurement at this urban site, which is likely to be influenced by the anthropogenic emissions from cooking and traffic.

Formatted: Subscript

The diurnal patterns of both BC_{ff} and BC_{bb} are shown alongside the PMF analysis in Figure 5a. Overall, the diurnal patterns of BC_{ff} and BC_{bb} are similar to the diurnal patterns of HOA and BBOA, respectively. The BC_{ff} component, represented by the red markers, exhibits pronounced peaks during the morning (6:00–9:00 am) and evening (5:00–9:00 pm) hours, corresponding to increased vehicular emissions during rush hours under the influence of a shallower planetary boundary layer. In contrast, the BC_{bb} component, depicted by the grey markers, shows relatively more consistent levels throughout the

day, with slight increases observed during the late evening (8:00–10:00 PM) and early morning (6:00–10:00 AM) hours.

There was a positive correlation between hourly BC and BBOA ($R^2 = 0.86$), BC_bb and BBOA ($R^2 = 0.86$), and BC and m/z 60 ($R^2 = 0.94$). Similarly, the HOA factor showed a linear relationship with BC ($R^2 = 0.73$), BC_ff ($R^2 = 0.61$), and m/z 57 ($R^2 = 0.95$) (see Figure S10 and Figure S11 in the supplemental information), indicating significant contributions from fossil fuel combustion and biomass burning to the total PM mass at the site.

While there is limited data on air pollution sources in other East African countries, our estimate that traffic emissions (HOA + BC_ff) contribute approximately 34–38% of Organic PM₁ is our results are consistent with the past filter-based source apportionment studies in the region. For example, in Mbarara, Uganda, a neighbouring country of Rwanda, elemental PM_{2.5} composition analysis and PMF revealed large contributions of traffic emissions and biomass burning, contributing 36% and 28% of the total PM_{2.5} mass, respectively (Onyango *et al.*, 2024). In Nairobi, Kenya, Gauta *et al.* (Gaita *et al.*, 2014) reported that traffic-related emissions accounted for 39% of the total PM_{2.5} mass.

In Western African countries, primary organic aerosols (POA) are also major contributors to PM_{2.5} mass. For instance, in Bamako, Mali, POA contributes 60–65% of the total PM_{2.5} mass. Similarly, in Dakar, Senegal, traffic emissions (including motor vehicle tailpipe emissions and resuspended road dust) account for 45–49% of the total PM_{2.5} mass loading (Environment, 2018; UN Environment, 2019).

3.5 Car-free day and community work initiatives' impact on PM-mass loading,

Different countries in Eastern Africa are implementing various measures to reduce PM emissions. For example, in the transportation sector, Rwanda has adopted electric mobility policies to reduce traffic-related PM emissions (Rwanda, 2021). A 2021 strategic paper on electric mobility adaptation by the Ministry of Infrastructure (Rwanda, 2021) outlines import and excise duty exemptions on electric vehicles (EVs), spare parts, investments in charging infrastructure, and access to high-occupancy vehicle lanes for EVs. Additionally, this strategy applies to a carbon tax on high-emission vehicles (old petrol-powered

Formatted: Font: Italic

Formatted: Font: Italic

Formatted: Font: (Default) Times New Roman, English (United Kingdom), Ligatures: None

Formatted: Default Paragraph Font, Font: (Default) Times New Roman, English (United Kingdom), Ligatures: None

Formatted: Font: (Default) Times New Roman, English (United Kingdom), Ligatures: None

Formatted: Font: (Default) Times New Roman, English (United Kingdom), Ligatures: None

Formatted: Font: (Default) Times New Roman, English (United Kingdom), Ligatures: None

Formatted: Subscript

Formatted: Font: (Default) Times New Roman, Italian (Italy), Ligatures: None

Formatted: Italian (Italy)

Formatted: Font: (Default) Times New Roman, Italian (Italy), Ligatures: None

Field Code Changed

Formatted: Subscript

Formatted: Subscript

Formatted: Subscript

Formatted: Font: Bold

Formatted: Level 2, Indent: Left: 0.25", Hanging: 0.25", Space Before: 12 pt, After: 12 pt, Line spacing: single, K with next, Tab stops: Not at 0.64" + 1.27" + 1.91" + 2.54" + 3.18" + 3.82" + 4.45" + 5.09" + 5.73" + 6.36" + 7.00" + 7.63" + 8.27" + 8.91" + 9.54" + 10.18"

Formatted: Font: Bold

vehicles) to discourage the use and importation of older and polluting vehicles. This strategy introduced tax exemptions on LPG to improve the affordability and adoption of EVs. To enhance compliance, the government of Rwanda has established motor vehicle inspection centers, requiring commercial vehicles to undergo biannual inspections and personal vehicles to be inspected annually. This initiative ensures that older, high-PM-emitting vehicles are monitored and regulated.

Rwanda also enforces car-free days in Kigali. These occur on two Sundays per month from 08:00 – 11:00 local time. Research by Subramanian et al. (Subramanian *et al.*, 2020) ~~shows~~ showed that Rwanda's car-free initiatives, such as car-free zones and car-free days, ~~can successfully reduce~~ reduced PM_{2.5} concentrations by ~~407~~-12 µg/m³ and black carbon (BC) by 1 µg/m³, demonstrating the effectiveness of vehicle emissions reductions in PM concentrations.

Rwanda also has a monthly community work initiative called Umuganda (Uwimbabazi, 2012). Umuganda occurs on the last Saturday every month from 08:00 – 11:00 local time. During Umuganda, there is a severe reduction in on-road traffic and commercial activities, as Rwandans use this time to focus on community cleaning and improvement projects.

Figures 6 and 7 examine the impacts of car-free days and Umuganda on PM₁ and PM_{2.5} concentrations. For this analysis, we divide the day into three broad time periods: during the car-free or Umuganda period (08:00 – 11:00), before the car-free or Umuganda period (0:00 – 07:00), and after (11:00 – 23:00). On car-free days, In the household energy sector, Rwanda is actively working to reduce PM emissions from biomass cooking by lowering biomass energy use from 85% to 44% (Republic of Rwanda, 2022). The 2022 ministerial guidelines on clean cooking technologies promote the adoption of LPG, biogas, liquid fuels, and improved clean burning cookstoves to reduce indoor and outdoor PM emissions from biomass combustion. Hence, the large-scale distribution of low-emission cookstoves to rural communities further supports this transition.

Formatted: Subscript

Formatted: Subscript

570 ~~For industrial PM emissions, the eastern African community developed different air emission Standards, for instance EAS 750:2010, EAC 751:2010, and EAC 1047:2022, which regulate ambient air, cement factory, and tailpipe emissions, respectively.~~

~~Most of the above initiative shows a promising reduction in air pollution, especially in PM mass concentration in this region.~~

(REMA, 2018)s

575 ~~For example, using the case of car free hours/day as discussed by Subramanian (Subramanian *et al.*, 2020) and the community work initiative, Umuganda, discussed by Uwimbabazi (Uwimbabazi, 2012), we compare the mean concentrations during 08:00–11:00 local time on car free Sundays with the same hours on other Sundays. We observe reductions of $4 \pm 1.5 \mu\text{g m}^{-3}$ in NR-PM₁ (-17% relative to regular Sundays) and $3 \pm 1 \mu\text{g m}^{-3}$ in PM_{2.5} (-6%, %) during the car-free period, which are This is smaller than the 7–12 $\mu\text{g m}^{-3}$ PM_{2.5} decreases reported by (Subramanian *et al.*, 2020) for the same city (Figure 5). The car-free days also had lower concentrations of PM₁ (until 17:00) and PM_{2.5} (until 21:00), compared to regular Sundays, after the car-free period ended.~~

580 In contrast, during the Umuganda period, we find an increase of $4 \mu\text{g m}^{-3}$ in total PM₁ (+13%) accompanied by a decrease of $4 \mu\text{g m}^{-3}$ in PM_{2.5} (-8%). ~~On Umuganda days, PM_{2.5} concentrations are reduced, compared to regular Saturdays, from 01:00 – 12:00, whereas PM₁ concentrations are higher during the morning from 06:00 – 09:00 am. The changes in PM₁ mass concentrations on car-free and Umuganda days are only about 10%, and the mass composition (the relative fraction of organics, BC, and inorganic ions) does not change significantly between these days and normal Saturdays and Sundays (Figure S17), except for a higher BC fractional contribution (mean 34.3%) during community work in the rainy season.~~

590 ~~During the car-free periods, concentrations of HOA and BBOA are both reduced relative to normal Sundays. HOA concentrations are 17% lower during car-free periods compared to normal Sundays, and, surprisingly, BBOA concentrations are 52% lower. In addition, the reduced emissions also reduce SOA formation, and OOA concentrations are 28% lower during the car-free period (Table S1, Figure S18). The~~

Formatted: Subscript

Formatted: Subscript

Formatted: Subscript

Formatted: Subscript

Formatted: Subscript

595 ~~reduced emissions during the car-free period also impact OOA concentrations when averaged across the~~
~~entire day, with daily average OOA concentrations on car-free days being 16% lower than on normal~~
~~Sundays. The impact of potential emission reductions is not apparent on Umuganda days. On those days,~~
~~both concentrations of PM₁ and OA components are higher than on normal Saturdays. Differences~~
~~between car-free and Umuganda likely reflect site characteristics (near-road PM_{2.5} vs. urban background~~
600 ~~PM₁) and neighborhood activity patterns around the monitors. For example, community work mornings~~
~~show higher HOA (+10%) and BBOA (+18%) compared with car-free hours (Figure S18). Neither~~
~~intervention produced a significant change in the relative contributions of OA sources to the overall PM₁~~
~~mass PMF-resolved organic-only PM₁ source strengths or a clear source shift across seasons in Kigali~~
~~(Figure S17). PM composition remained broadly similar between the two interventions, except for a~~
605 ~~higher BC fractional contribution (mean 34.3%) during community work in the rainy season, likely~~
~~reflecting stronger wet deposition of other PM components relative to BC.~~

Formatted: Subscript

Seasonally, ~~the wet-to-dry season ratio of relative changes indicates that car-free day interventions are~~
~~more effective in the dry season, with lower ratios across all species (0.84–0.97), reflecting higher~~
610 ~~baseline concentrations and stronger relative reductions. In contrast, community work events show higher~~
~~wet-to-dry ratios (1.02–1.25), particularly for household and biomass-related species (HOA and BBOA),~~
~~indicating a stronger relative impact of domestic emissions during the wet season. (see Table 1 in SI).~~

615 ~~Overall, car-free suppresses secondary inorganics—NO₃–38.7%, NH₄–25%, SO₄–23%, Cl⁻–23%—~~
~~via reduced vehicle NO_x and SO₂, but coincides with increases in primary/organic markers (HOA~~
~~+64.6%, BBOA +35.5%, OOA +36.8%) and BC +7.7% (BC_{ff} +5.5%, BC_{BB} +10.2%). Umuganda~~
~~reduces traffic BC –13.6% (BC_{ff} –15.8%, BC_{BB} –11.7%) yet elevates HOA +38.5% and sulfate,~~
~~yielding a net PM₁ rise (+19.4%).~~

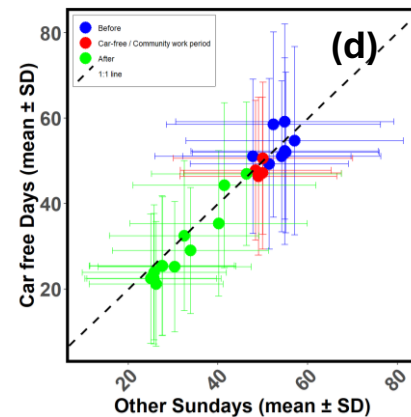
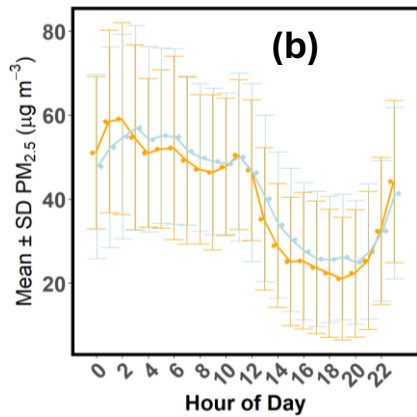
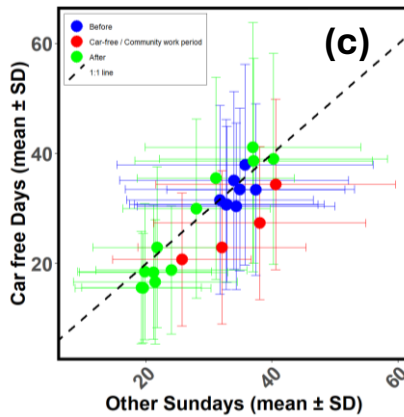
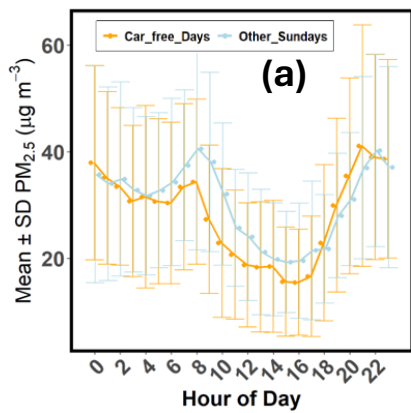
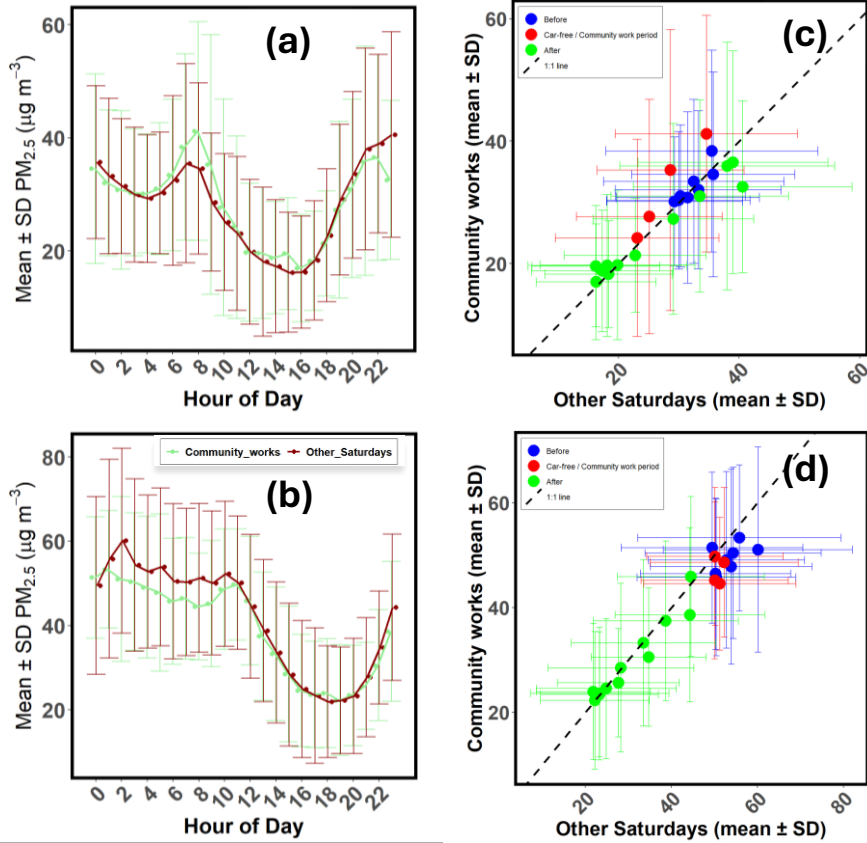


Figure 56: Impact of limiting vehicle movement on Sundays in Kigali on PM_1 and $PM_{2.5}$. Panels (a) and (b) show the hourly average diurnal patterns for PM_1 and $PM_{2.5}$, respectively, across 25 car-free Sundays and 28 regular Sundays from April 2023 to May 2024. Panels (c) and (d) show scatter plots for PM_1 and $PM_{2.5}$ for comparing both car-free day and regular Sundays.



§30 **Figure 56:** Impact of community work on every last Saturday of each month in Kigali on PM₁ and PM_{2.5}. Panels (a) and (b) show the hourly average patterns for PM₁ and PM_{2.5}, respectively, across 13 community works and 40 regular Saturdays from April 2023 to May 2024. Panels (c) and (d) show scatter plots for PM₁ and PM_{2.5} for the same period for the community works vs regular Saturday.

635 **4. Conclusion**

The measurements presented here show that PM_{10} in Kigali is impacted by high primary emissions of BC and OA, along with strong secondary production of OA and nitrate. This is consistent with Rwanda being a nation with a relatively old and higher-emitting vehicle fleet, high usage of solid biomass fuels for cooking, and high solar insolation.

640 The transport sector in Rwanda is dominated by old vehicles imported from other countries. Rwanda's registered motor vehicles, including two-wheeled taxis ("motos") but excluding security organs and government vehicles, totaled 191,015 in 2017 and 264,524 in 2020. Of these, only 15% were new vehicles, while the remaining 85% were imported used vehicles, 95% of which were manufactured before 2005 (Niyibizi *et al.*, 2015; Environment, 2018; REMA, 2018; UN Environment, 2019; STATISTICAL, 645 2021). While we do not have specific emissions measurements for the vehicle fleet, the ambient data presented here suggest that vehicles in Rwanda are high emitters of both BC and OA. Additionally, these vehicle emissions contribute precursor vapors for SOA production.

In Rwanda, as in most Eastern African countries, biomass (e.g., charcoal, wood, and biogas derived from waste materials) accounts for more than 80% of total energy consumption (MINEFRA, 2018b). Our 650 analyses show that biomass burning, even in urban Kigali, contributes 23% of OA and 41% of BC. Some of the OA and BC attributable to biomass burning are emitted locally, as evidenced by the morning and evening peaks in BBOA and BC_{bb}. However, the morning and evening enhancements in BBOA and BC_{bb} are relatively small, and there are also high concentrations of BBOA and BC_{bb} overnight (e.g., from 12:00 am to 4:00 am). Anderson *et al.* (2020) and Kirago *et al.* (2022) measured a mean concentration 655 of ~0.5 mg m⁻³ at the remote Rwanda Climate Observatory; this BC was 91% attributed to biomass burning. If we assume that the Rwanda Climate Observatory measurements represent a regional concentration of biomass-related BC, then about one-third of the biomass-burning BC in Kigali is from regional sources.

660 [In the household energy sector, Rwanda is actively working to reduce PM emissions from biomass cooking by lowering biomass energy use from 85% to 44% \(Republic of Rwanda, 2022\). The 2022 ministerial guidelines on clean cooking technologies promote the adoption of LPG, biogas, liquid fuels,](#)

Formatted: Subscript

665 [and improved clean-burning cookstoves to reduce indoor and outdoor PM emissions from biomass combustion. Hence, the large-scale distribution of low-emission cookstoves to rural communities further supports this transition](#)(Republic of Rwanda, 2022).[For industrial PM emissions, the eastern African community developed different air emission standards, for instance EAS 750:2010, EAC 751:2010, and EAC 1047:2022, which regulate ambient air, cement factory, and tailpipe emissions, respectively](#)(Rwanda Standard Board, 2010; Rwanda Standard Boards, 2011).

670 There are modest seasonal variations in PM_{10} mass concentrations, with about 10% higher concentrations of both PM_{10} and $PM_{2.5}$ during the dry season. Source apportionment analysis of both OA and BC shows smaller variations in source strengths across seasons. This suggests that the main reason for higher PM concentrations in the dry seasons is a reduction in wet deposition, rather than increased source strengths. However, there remains the possibility that there exist season-dependent shifts in emission sources. For example, the rainy seasons have a higher fraction of BC from biomass-burning sources than the dry seasons. This may be due to biomass burning for agricultural residue disposal or because of transported emissions from open burning in the northern and southern regions of Rwanda ([Andersson et al., 2020](#)).
675 ~~(Andersson et al. 2020b).~~

680 ~~While regional cooperation frameworks exist, weak enforcement remains a major challenge in addressing transboundary PM pollution. Strengthening compliance requires the establishment of a legally binding regional agreement with clear PM reduction targets and penalties for non-compliance. Prioritizing a joint regional PM monitoring network would enable real-time tracking of PM sources, supporting evidence-based enforcement. Additionally, empowering cross-border regulatory bodies to conduct independent audits, inspections, and enforcement actions is essential to ensure compliance with PM standards. Strengthening regional funding mechanisms for clean energy transitions and emission reduction projects targeting PM sources, such as biomass burning, industrial activities, and vehicle emissions, would provide~~

Formatted: Subscript

Formatted: Subscript

Formatted: Subscript

~~critical financial support while fostering collaboration among governments, industries, and environmental agencies across the region.~~

~~This study shows that short-term interventions, such as car-free days and community works (Uganda), can effectively reduce traffic-related emissions. Combined with the long-term decline in traffic emissions, these findings emphasize the importance of pairing social initiatives with sustained emission control strategies, including vehicle inspection enforcement, fleet electrification, and cleaner household energy. By providing baseline source apportionment data, this study supports evidence-based policy design and highlights the need for regular monitoring, stronger enforcement, and regional cooperation to address transboundary sources. Together, these actions can deliver lasting improvements in urban air quality and public health across the region.~~

Formatted: English (United Kingdom)

Formatted: English (United Kingdom)

Formatted: English (United Kingdom)

Formatted: English (United Kingdom)

Formatted: Default Paragraph Font, Font: (Default) +Bod (Aptos), English (United Kingdom), Ligatures: Standard + Contextual

Formatted: Normal, Justified, Line spacing: 1.5 lines, Adj space between Asian text and numbers, Tab stops: 0.64", Left + 1.27", Left + 1.91", Left + 2.54", Left + 3.18", Left + 3.82", Left + 4.45", Left + 5.09", Left + 5.73", Left + 6.36", Left + 7", Left + 7.63", Left + 8.27", Left + 8.91", Left + 9.54", Left + 10.18", Left

Formatted: Font: (Default) Times New Roman, 12 pt, Bold, Font color: Black, English (United Kingdom), Kern at 16 pt, Ligatures: None

Formatted: Indent: First line: 0"

Formatted: Font: (Default) Times New Roman, English (United Kingdom), Ligatures: None

Formatted: Font: (Default) Times New Roman, Not Bold, English (United Kingdom), Ligatures: None

5. Data availability.

All data presented in this work can be obtained by directly contacting the corresponding author at apresto@andrew.cmu.edu upon request. Data will also be posted to a publicly available server (<https://kilthub.cmu.edu/>) upon final acceptance.

6. Competing interests.

The authors declare that they have no conflict of interest.

7. Author contribution

The experimental design was done by AAP, ALR, and TH. Data collection was carried out by AAP and TH. TH performed the data analysis and compiled the instrumental data. TH, AAP, and ALR wrote the

710 paper, with all authors contributing significantly to the interpretation of the results, discussions, and
finalization of the paper.

8. Acknowledgments

This work was funded by National Science Foundation Grants 2420751 and 2020666 and the Steinbrenner
Institute for Environmental Education and Research at Carnegie Mellon University. We thank the Rwanda
715 Space Agency and Earth and Space Science Division for providing the Q-ACSM and AE33 instrument
data used in this study. We also extend our gratitude to the Rwanda Space Agency technical team (Dr.
Ntwali Didier, Mr. Olivier Shyaka, Mr. Gaston Munyampundu, Mr. Jacques Nshuti, Mr. Eric Byiringiro,

and Mr. Emmanuel Iradukunda) from the Rwanda Climate Observatory Project for their technical support and assistance with instrument operation.

720
725
730
735
740
745

9. References

- AirNow (2025) *Air pollution measurement*. Available at: <https://www.airnow.gov/> last accesses 2024-06-05 (Accessed: June 5, 2024).
- 755 Andersson, A. *et al.* (2020) “Seasonal source variability of carbonaceous aerosols at the Rwanda Climate Observatory,” *Atmospheric Chemistry and Physics*, 20(8), pp. 4561–4573. Available at: <https://doi.org/10.5194/acp-20-4561-2020>.
- Brito, J. *et al.* (2018) “Assessing the role of anthropogenic and biogenic sources on PM1 over southern West Africa using aircraft measurements,” *Atmospheric Chemistry and Physics*, 18(2), pp. 757–772. Available at: <https://doi.org/10.5194/acp-18-757-2018>.
- 760 Budisulistiorini, S.H. *et al.* (2013) “Real-time continuous characterization of secondary organic aerosol derived from isoprene epoxydiols in downtown Atlanta, Georgia, using the aerodyne aerosol chemical speciation monitor,” *Environmental Science and Technology*, 47(11), pp. 5686–5694. Available at: <https://doi.org/10.1021/es400023n>.
- Day, D.A. *et al.* (2022) “A systematic re-evaluation of methods for quantification of bulk particle-phase organic nitrates using real-time aerosol mass spectrometry,” *Atmospheric Measurement Techniques*, 15(2), pp. 459–483. Available at: <https://doi.org/10.5194/amt-15-459-2022>.
- 765 Dewitt, H.L. *et al.* (2019) “Seasonal and diurnal variability in O3, black carbon, and CO measured at the Rwanda Climate Observatory,” *Atmospheric Chemistry and Physics*, 19(3), pp. 2063–2078. Available at: <https://doi.org/10.5194/acp-19-2063-2019>.
- Dhammapala, R. (2019) “Analysis of fine particle pollution data measured at 29 US diplomatic posts worldwide,” *Atmospheric Environment*, 213, pp. 367–376. Available at: <https://doi.org/10.1016/j.atmosenv.2019.05.070>.
- 770 Drew R. Gentner (2016) “Review of Urban Secondary Organic Aerosol Formation from Gasoline and Diesel Motor Vehicle Emissions,” in: ACS publisher. Available at: <https://doi.org/10.1021/acs.est.6b04509>.
- Engeln, A.V. and Teixeira, J. (2013) “A planetary boundary layer height climatology derived from ECMWF reanalysis data,” *Journal of Climate*, 26(17), pp. 6575–6590. Available at: <https://doi.org/10.1175/JCLI-D-12-00385.1>.
- 775 Environment, U.N. (2018) *Kigali City Air Quality Policy and Regulatory Situational Analysis A report published by UN Environment in collaboration with Environmental Compliance Institute*.
- Fisher, S. *et al.* (2021) “Air pollution and development in Africa: impacts on health, the economy, and human capital,” *The Lancet Planetary Health*, 5(10), pp. e681–e688. Available at: [https://doi.org/10.1016/S2542-5196\(21\)00201-1](https://doi.org/10.1016/S2542-5196(21)00201-1).

- Gahungu, P. and Kubwimana, J.R. (2022) "Trend analysis and forecasting air pollution in Rwanda." Available at: <http://arxiv.org/abs/2205.10024>.
- 780 Gaita, S.M. *et al.* (2014) "Source apportionment and seasonal variation of PM_{2.5} in a sub-Saharan African city: Nairobi, Kenya," *Atmospheric Chemistry and Physics*, 14(18), pp. 9977–9991. Available at: <https://doi.org/10.5194/acp-14-9977-2014>.
- GBD (2024) *Global Burden diseases*, <https://vizhub.healthdata.org/gbd-compare/#>.
- He, X. *et al.* (2022) "Comprehensive chemical characterization of gaseous I/SVOC emissions from heavy-duty diesel vehicles using two-dimensional gas chromatography time-of-flight mass spectrometry," *Environmental Pollution*, 305. Available at: <https://doi.org/10.1016/j.envpol.2022.119284>.
- 785 Health Effects Institute (2022) "The State of Air Quality and Health Impacts in Africa.," p. PP. 10-20.
- Health Effects Institute (2023) "The State of Air Quality and Health Impacts in Africa. A Report from the State of Global Air Initiative. Boston, MA:Health Effects Institute.," p. PP. 10-30.
- Huffman, J.A. *et al.* (2005) "Design, modeling, optimization, and experimental tests of a particle beam width probe for the aerodyne aerosol mass spectrometer," *Aerosol Science and Technology*, 39(12), pp. 1143–1163. Available at: <https://doi.org/10.1080/02786820500423782>.
- 790 Kalisa, E. *et al.* (2018) "Characterization and Risk Assessment of Atmospheric PM_{2.5} and PM₁₀ Particulate-Bound PAHs and NPAHs in Rwanda, Central-East Africa," *Environmental Science and Technology*, 52(21), pp. 12179–12187. Available at: <https://doi.org/10.1021/acs.est.8b03219>.
- 795 Kalisa, E. *et al.* (2025) "Natural experiments in urban air quality: lessons from car-free days and COVID-19 lockdowns in Kigali, Rwanda," *Cities and Health* [Preprint]. Available at: <https://doi.org/10.1080/23748834.2025.2468017>.
- Kalisa, E. and Adams, M. (2022) "Population-scale COVID-19 curfew effects on urban black carbon concentrations and sources in Kigali, Rwanda," *Urban Climate*, 46. Available at: <https://doi.org/10.1016/j.uclim.2022.101312>.
- Kigali city (2024) *Kigali city population*, <https://www.kigalicity.gov.rw/about/overview>.
- 800 Kigali City (2024) "Kigali city population(last accessed: Nov 2024).," <https://www.kigalicity.gov.rw/about/overview>.
- Kirago, L. *et al.* (2022) "Atmospheric Black Carbon Loadings and Sources over Eastern Sub-Saharan Africa Are Governed by the Regional Savanna Fires," *Environmental Science and Technology*, 56(22), pp. 15460–15469. Available at: <https://doi.org/10.1021/acs.est.2c05837>.
- 805 Lanz, V.A. *et al.* (2007) *Source apportionment of submicron organic aerosols at an urban site by factor analytical modelling of aerosol mass spectra*, *Atmos. Chem. Phys*, pp. 1503–1522. Available at: www.atmos-chem-phys.net/7/1503/2007/.
- Liu, P.S.K. *et al.* (2007) "Transmission efficiency of an aerodynamic focusing lens system: Comparison of model calculations and laboratory measurements for the aerodyne aerosol mass spectrometer," *Aerosol Science and Technology*, 41(8), pp. 721–733. Available at: <https://doi.org/10.1080/02786820701422278>.
- Magee Scientific (2017) *Aethalometer Model AE33 User Manual*. Available at: www.aerosol.eu.

- 810 Matthew, B.M., Middlebrook, A.M. and Onasch, T.B. (2008) "Collection efficiencies in an aerodyne aerosol mass spectrometer as a function of particle phase for laboratory generated aerosols," *Aerosol Science and Technology*, 42(11), pp. 884–898. Available at: <https://doi.org/10.1080/02786820802356797>.
- McFarlane, C. *et al.* (2021) "First measurements of ambient pm2.5 in kinshasa, democratic republic of congo and brazzaville, republic of congo using field-calibrated low-cost sensors," *Aerosol and Air Quality Research*, 21(7). Available at: <https://doi.org/10.4209/aaqr.200619>.
- 815 Meteo_Rwanda, M. (2025) "Climatology of eastern Africa(last accessed: Jan 2025).," <https://www.meteorwanda.gov.rw/index.php?id=2>.
- Miller, J. and Jin, L. (2018) *Global progress toward soot-free diesel vehicles in 2018*. Available at: www.theicct.org.
- MINEFRA (2015) *Republic Of Rwanda Ministry Of Infrastructure Rwanda Energy Policy*. Rwanda: Mifotra. Available at: <https://www.mininfra.gov.rw> (Accessed: October 10, 205 AD).
- 820 MINEFRA (2018a) *Energy sector strategic plan. 2019/19-2023/24*. Rwanda. Available at: <https://www.mininfra.gov.rw>.
- MINEFRA (2018b) *Republic Of Rwanda Ministry Of Infrastructure Energy Sector Strategic Plan*. Rwanda: Mifotra. Available at: <https://www.mininfra.gov.rw>.
- Mkoma, S.L. *et al.* (2009) "Characterisation of PM10 atmospheric aerosols for the wet season 2005 at two sites in East Africa," *Atmospheric Environment*, 43(3), pp. 631–639. Available at: <https://doi.org/10.1016/j.atmosenv.2008.10.008>.
- 825 Monitor, G.E. (2025) "worldwide coal plants," <https://globalenergymonitor.org/projects/global-coal-plant-tracker/tracker/>.
- Ndamuzi, E. *et al.* (2024) "Modeling and Characterization of Fine Particulate Matter Dynamics in Bujumbura Using Low-Cost Sensors," *Journal of Applied Mathematics and Physics*, 12(01), pp. 256–267. Available at: <https://doi.org/10.4236/jamp.2024.121020>.
- 830 Ng, N.L. *et al.* (2011) "Real-time methods for estimating organic component mass concentrations from aerosol mass spectrometer data," *Environmental Science and Technology*, 45(3), pp. 910–916. Available at: <https://doi.org/10.1021/es102951k>.
- Nicholson, S.E. (2017) "Climate and climatic variability of rainfall over eastern Africa," *Reviews of Geophysics*, 55(3), pp. 590–635. Available at: <https://doi.org/10.1002/2016RG000544>.
- 835 NIS Rwanda (2021) *Republic of Rwanda Statistical Year book*. Available at: <http://www.statistics.gov.rw>.
- Niyibizi, A. *et al.* (2015) "Quantification of Air Pollution in Kigali City and Its Environmental and Socio-Economic Impact in Rwanda," *American Journal of Environmental Engineering*, 5, pp. 106–119. Available at: <https://doi.org/10.5923/j.ajee.20150504.03>.
- 840 Nyeki, S. *et al.* (1998) "The background aerosol size distribution in the free troposphere: An analysis of the annual cycle at a high-alpine site," *Journal of Geophysical Research Atmospheres*, 103(D24), pp. 31749–31761. Available at: <https://doi.org/10.1029/1998JD200029>.
- Onyango, S. *et al.* (2024) "Ambient PM2.5 Temporal Variation and Source Apportionment in Mbarara, Uganda," *Aerosol and Air Quality Research*, 24(4). Available at: <https://doi.org/10.4209/aaqr.230203>.

- openaq (2025) "Air pollution monitoring map," <https://explore.openaq.org/?parameter=pm25#1/24.6/55.8>.
- 845 Oregon USA WaveMetrics (2024) "Igor pro wave matrix(last accessed: Nov 2024)," <https://www.wavemetrics.com/downloads/current/Igor%20Pro%209>.
- Paatero, P. and Tapper, U. (1994) "Positive matrix factorization: A non-negative factor model with optimal utilization of error estimates of data values," *Environmetrics*, 5(2), pp. 111–126. Available at: <https://doi.org/10.1002/env.3170050203>.
- 850 REMA (2018) *Rwanda Environment Management Authority Inventory of Sources of Air Pollution in Rwanda Determination of Future Trends and Development of a National Air Quality Control Strategy Rwanda Environment Management Authority*.
- Republic of Rwanda (2022) *Ministerial Guidelines for Clean Cooking Technologies*. Available at: <https://www.mininfra.gov.rw> last accessed 05/09/2025.
- Rwanda, R. of (2021) *Electric mobility adaptation in Rwanda*. Open 2043/20–2024/27. Rwanda: MINEFRA. Available at: <https://www.mininfra.gov.rw>.
- 855 Rwanda Standard Board, R.S. (2010) "Emission to the air by cement factories." Rwanda: ISO. Available at: https://portal.rsb.gov.rw/webstore_preview.php?id=ODY3RkJrTndaM0EzcA/ last accessed Sep 2025 (Accessed: September 5, 2025).
- 860 Rwanda Standard Boards (2011) "Air quality Specification." Available at: https://www.portal.rsb.gov.rw/webstore_view.php?i=ODIyODAxRkJrTndaM0EzcA/ last accessed Sep 2025 (Accessed: September 2, 2025).
- Sandradewi, J. *et al.* (2008) "Using aerosol light absorption measurements for the quantitative determination of wood burning and traffic emission contribution to particulate matter," *Environmental Science and Technology*, 42(9), pp. 3316–3323. Available at: <https://doi.org/10.1021/es702253m>.
- 865 Singh, A. *et al.* (2021) "Air quality assessment in three east african cities using calibrated low-cost sensors with a focus on road-based hotspots," *Environmental Research Communications*, 3(7). Available at: <https://doi.org/10.1088/2515-7620/ac0e0a>.
- Sitati, C.N. *et al.* (2022) "A street-level assessment of greenhouse gas emissions associated with traffic congestion in the city of Nairobi, Kenya," *Clean Air Journal*, 32(1). Available at: <https://doi.org/10.17159/caj/2022/32/1.12546>.
- 870 Smithsonian Institute (2025) "Global Volcanism Program, 2024. Report on Nyiragongo (DR Congo) (Sennert, S, ed.). Weekly Volcanic Activity Report, 3 July-9 July 2024. Smithsonian Institution and US Geological Survey." Available at: https://volcano.si.edu/volcanolist_countries.cfm?country=Rwanda (Accessed: February 15, 2025).
- STATISTICAL, R.B.O. (2021) *Republic of Rwanda Statistical year book 2021*. Available at: <http://www.statistics.gov.rw>.
- Subramanian, R. *et al.* (2020) "Air pollution in Kigali, Rwanda: spatial and temporal variability, source contributions, and the impact of car-free Sundays," *Clean Air Journal*, 30(2), pp. 1–15. Available at: <https://doi.org/10.17159/caj/2020/30/1.8023>.
- 875 Taghian, G. *et al.* (2024) "The Burden of Cardiovascular Disease from Air Pollution in Rwanda," *Annals of Global Health*, 90(1). Available at: <https://doi.org/10.5334/aogh.4322>.

Tefera, W. *et al.* (2021) "Source apportionment of fine organic particulate matter (PM_{2.5}) in central Addis Ababa, Ethiopia," *International Journal of Environmental Research and Public Health*, 18(21). Available at: <https://doi.org/10.3390/ijerph182111608>.

880 Teledyne (2016) *Model T640 PM Mass Monitor*. Available at: <http://www.teledyne-api.com/>.

Ulbrich, I.M. *et al.* (2009) "Interpretation of organic components from Positive Matrix Factorization of aerosol mass spectrometric data," *Atmos. Chem. Phys.* [Preprint].

885 Ulbrich, I.M., H., A., Lechner, M., and Jimenez, J.L. (2025) *AMS Spectral Database (Unit Mass Resolution)*, <http://cires.colorado.edu/jimenez-group/AMSsd/> last accessed Sep 2025. Available at: <http://cires.colorado.edu/jimenez-group/AMSsd/>.

UN Environment, R. (2019) *Kigali City Air Quality Policy and Regulatory Situational Analysis A report published by UN Environment in collaboration with Environmental Compliance Institute*. UN, pp. 1–14.

890 UNFCCC_Rwanda (2021) *REPUBLIC OF RWANDA Rwanda's First Biennial Update Report Under the United Framework Convention on Climate Change (UNFCCC) REPUBLIC OF RWANDA Rwanda's First Biennial Update Report Under the United Nations Framework Convention on Climate Change (UNFCCC)*. Available at: www.rema.gov.rw.

Uwimbabazi, P. (2012) *An Analysis of Umuganda: the Policy and Practice of Community Work in Rwanda*. PhD Thesis. KwaZulu-Natal.

895 Werden, B.S. *et al.* (2023) "Submicron Aerosol Composition and Source Contribution across the Kathmandu Valley, Nepal, in Winter," *ACS Earth and Space Chemistry*, 7(1), pp. 49–68. Available at: <https://doi.org/10.1021/acsearthspacechem.2c00226>.

WHO (2025) "Air pollution data portal(last accessed: Feb 2025)," <https://www.who.int/data/gho/data/themes/air-pollution>. Available at: <https://www.who.int/data/gho/data/themes/air-pollution>.

World Bank (2021) *Rwanda Climate risk country profile*. Available at: www.worldbank.org.

900 Zhang, Q. *et al.* (2011) "Understanding atmospheric organic aerosols via factor analysis of aerosol mass spectrometry: A review," *Analytical and Bioanalytical Chemistry*, 401(10), pp. 3045–3067. Available at: <https://doi.org/10.1007/s00216-011-5355-y>.